

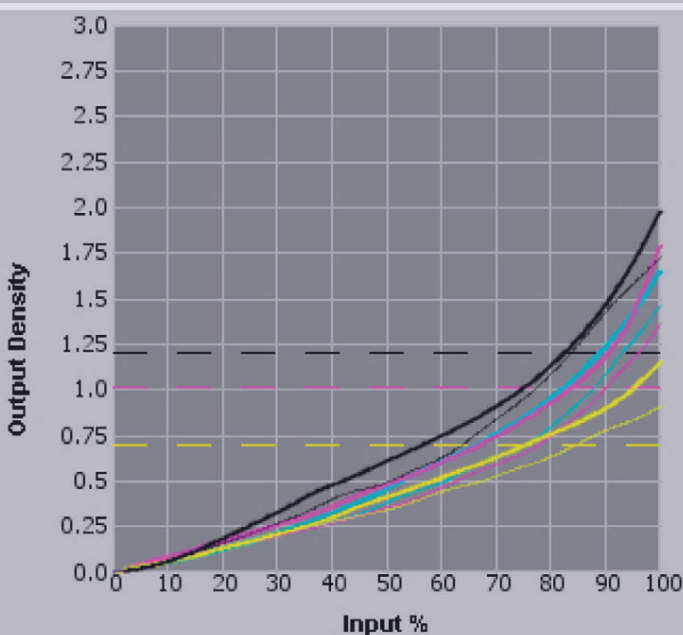
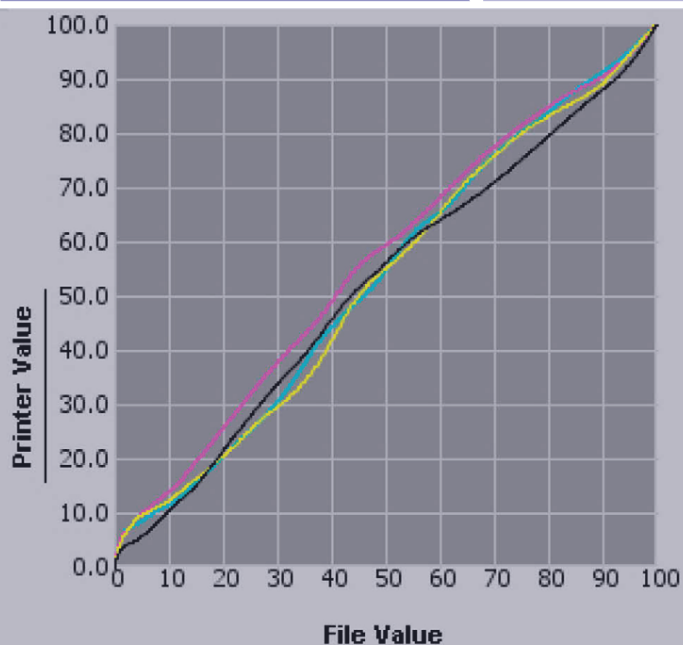


University of Novi Sad  
Faculty of Technical Sciences  
DEPARTMENT OF GRAPHIC  
ENGINEERING AND DESIGN

Volume **12**  
Number **1**  
March **2021**

# JGED

JOURNAL OF GRAPHIC  
ENGINEERING AND DESIGN

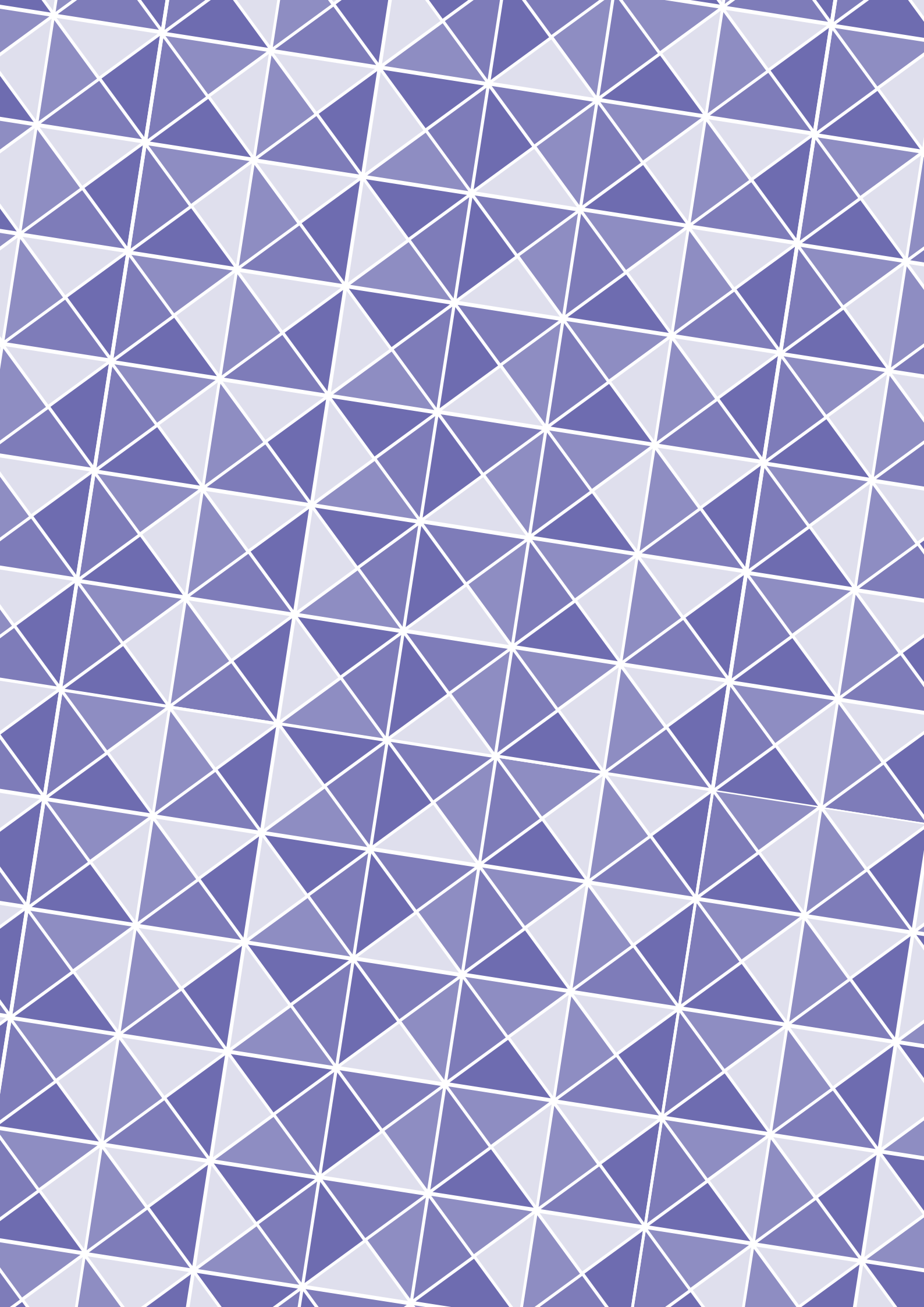


Online Workflow Puzzle  
Thomas Hoffman-Walbeck, Richard Adams

An investigation on skeleton-based  
top-down modelling approaches  
of complex industrial product  
Claudio Ciaccioli, Anna Eva Morabito

Aiming for G7 Master Compliance  
through a Color Managed Digital  
Printing Workflow (CMDPW):  
Comparison of Compliance with  
Output Device Profile (ODP) vs.  
Device Link Profile (DLP)  
Haji Naik Dharavath

Optimization of flexographic  
print properties on ecologically  
favorable paper substrates  
Tamara Tomašegović, Jesenka Pibernik, Sanja  
Mahović Poljaček, Anđela Mađžar



# JGED

JOURNAL OF GRAPHIC  
ENGINEERING AND DESIGN

1/2021

Volume 12, Number 1, March 2021.

**Published by**

UNIVERSITY OF NOVI SAD, SERBIA  
Faculty of Technical Sciences  
Department of Graphic Engineering and Design

## PUBLISHED BY



University of Novi Sad  
Faculty of Technical Sciences  
DEPARTMENT OF GRAPHIC  
ENGINEERING AND DESIGN

### Address:

Faculty of Technical Sciences,  
Department of Graphic  
Engineering and Design,

Trg Dositeja Obradovića 6  
21000 Novi Sad, Serbia

### Telephone numbers:

+381 21 485 26 20  
+381 21 485 26 26  
+381 21 485 26 21

### Fax number:

+381 21 485 25 45

### Email:

jged@uns.ac.rs

### Web address:

www.grid.uns.ac.rs/jged

Frequency: 4 issues per year

Printing: Faculty of Technical Sciences,  
Department of Graphic Engineering and Design

Circulation: 200

Electronic version of journal available on  
[www.grid.uns.ac.rs/jged](http://www.grid.uns.ac.rs/jged)

E-ISSN 2217-9860

The journal is abstracted/indexed  
in the Scopus and Directory of Open Access Journals



CIP - Katalogizacija u publikaciji  
Biblioteka Matice srpske, Novi Sad  
655

JGED : Journal of Graphic Engineering and Design /  
editor Dragoljub Novaković. - Vol. 1, No. 1 (nov. 2010) -  
Sciences, Department of Graphic Engineering and  
Design,  
2010-. 30 cm  
Četiri puta godišnje  
ISSN 2217-379X  
COBISS.SR-ID 257662727



© 2021 Authors. Published by the University of Novi Sad, Faculty of  
Technical Sciences, Department of Graphic Engineering and Design. All  
articles are an open access articles distributed under the terms and con-  
ditions of the Creative Commons Attribution license 3.0 Serbia (<http://creativecommons.org/licenses/by/3.0/rs/>).

## EDITORS

**Dragoljub Novaković**, University of Novi Sad, Novi Sad, Serbia

**Nemanja Kašiković**, University of Novi Sad, Novi Sad, Serbia

## EDITORIAL BOARD

**Thomas Hoffmann-Walbeck**

HDM Stuttgart, Stuttgart, Germany

**Rafael Huertas**

University of Granada, Granada, Spain

**Joanna Ewa Izdebska**

Warsaw University of Technology, Warsaw, Poland

**Igor Majnarić**

University of Zagreb, Zagreb, Croatia

**Branko Milosavljević**

University of Novi Sad, Novi Sad, Serbia

**Deja Muck**

University of Ljubljana, Ljubljana, Slovenia

**László Koltai**

Óbuda University, Budapest, Hungary

**Anastasios E. Politis**

Hellenic Union of Graphic Arts and Media Technology Engineers-  
HELGRAMED, Athens, Greece

**Miljana Prica**

University of Novi Sad, Novi Sad, Serbia

**Iskren Spiridonov**

University of Chemical Technology and Metallurgy,  
Sofia, Bulgaria

**Mladen Stančić**

University of Banja Luka, Banja Luka, Bosnia and Herzegovina

**Tomáš Syrový**

University of Pardubice, Pardubice, Czech Republic

**Gojko Vladić**

University of Novi Sad, Novi Sad, Serbia

**Thomas Sabu**

Mahatma Gandhi University, Kottayam, India

**Jonas Malinauskas**

Vilnius College of Technologies and Design, Vilnius, Lithuania

**Roberto Pašić**

UKLO University St. Climent Ohridski, Bitola, North Macedonia

**Behudin Mešić**

SCION, Rotorua, New Zealand

**Arif Özcan**

Marmara University, Istanbul, Turkey

**Vladan Končar**

ENSAIT, Roubaix, France

**Catarina Silva**

Polytechnic Institute of Cávado and Ave (IPCA), Barcelos, Portugal

**Michal Čeppan**

Slovak University of Technology in Bratislava, Slovakia

**Tim C Claypole**

Swansea University, Swansea, United Kingdom

**Alexandra Pekarovicova**

Western Michigan University, Kalamazoo, USA

**Panagiotis Kyratsis**

University of Western Macedonia, Kozani, Greece

**Jason Lisi**

Ryerson University, Toronto, Canada

**Peter Nussbaum**

Norwegian University of Science and Technology, Gjøvik, Norway

### Art Director

Uroš Nedeljković

### Layout design

Bojan Banjanin

### Journal cover design

Nada Miketić

# JOURNAL OF GRAPHIC ENGINEERING AND DESIGN

Volume 12, Number 1, March 2021.

## Contents


- 5 **Online Workflow Puzzle**  
*Thomas Hoffman-Walbeck, Richard Adams*
- 11 **An investigation on skeleton-based top-down modelling approaches of complex industrial product**  
*Claudio Ciaccioli, Anna Eva Morabito*
- 23 **Aiming for G7 Master Compliance through a Color Managed Digital Printing Workflow (CMDPW): Comparison of Compliance with Output Device Profile (ODP) vs. Device Link Profile (DLP)**  
*Haji Naik Dharavath*
- 37 **Optimization of flexographic print properties on ecologically favorable paper substrates**  
*Tamara Tomašegović, Jesenka Pibernik, Sanja Mahović Poljaček, Anđela Madžar*



# Online Workflow Puzzle

## ABSTRACT

*We are presenting an online workflow puzzle, which runs in a browser. The player can put together puzzle pieces to pre-defined production chains. Extensive online help supports the player in laying out the puzzle pieces correctly. The puzzle is based on the process-resource model, which is also the basis of the Job Definition Format. This paper explains the game as well as implementation strategy.*

Thomas Hoffman-Walbeck<sup>1</sup>   
Richard Adams<sup>2</sup>

<sup>1</sup> Stuttgart Media University,  
Stuttgart, Germany

<sup>2</sup> Ryerson University,  
Toronto, Canada

*Corresponding author:  
Thomas Hoffman-Walbeck  
e-mail: [hoffmann@hdm-stuttgart.de](mailto:hoffmann@hdm-stuttgart.de)*

## KEY WORDS

workflow, online game, JavaScript, HTML, jQuery, JDF

First received: 1.6.2020.

Revised: 4.9.2020.

Accepted: 7.9.2020.

## Introduction

A Print Service Provider (PSP) needs many experts in order to accomplish all the different production processes, which are necessary for manufacturing a print product. Those experts usually have a deep knowledge in their special fields. For example, to determine the width of the spine for a hard cover book sounds easy at the first glance, however, it often requires a lot of expertise and experience. On the other hands, project and production manager do not need to know all details of each production process. They should be able to pre-define the necessary production steps, their sequence, their upfront requirements and their outcomes. This reflects the old mantra of specialists and generalists.

Conducting student projects in graphical departments at universities, we noticed that even students tend to specialize very much. Some of them are interested in product design (only), others in Prepress, Press or Postpress. That is, in practical group proj-

ects most students like to pick their favorite topic, which they know best already. In the end, it is hard for most of them, to outline a production overview.

Several years ago, we created different versions of paper-based gaming cards for different processes: In lab classes, the students laid the cards on a table in an ordered manner displaying a specific production workflow. The students paired up in small groups in order to stimulate a discussion about the solution.

Increasing production automation definitely is key in the Graphical Industry. There are two very different ways to accomplish that:

- a. automating individual processes or
- b. automating the workflow

Automation of machines falls into category a). That is, robots, cobots and production equipment that, for example, shortens make-ready times.

---

Software algorithm in Prepress for automating an individual task we also subsume under a).

Automation of class b) has two variants. One is of purely organizational (e.g. by determining who is supposed to transmit at what time imaged plates to the offset press); the other one has more of an IT aspect: Devices and software modules sharing information to make sure that each process gets all the required resources that they need for executing in time. There are still many optimization potentials in this. It is the area of the Job Definition Format (CIP4, 2020a), where product descriptions and production details are sent to several devices so that those can use them for an (automatic) execution of a process. Often, this is called an “integration” of processes.

JDF employs the process-resource model for the product description. This is also true for XJDF (CIP4, 2020b), but to a somewhat lesser extent. A process is an activity like printing or folding. Mostly, a process requires input resources for execution and generates one or more output resources. In general, a resource is either some physical object (like plates or paper) or some electronic/conceptual entities (like PDF pages, parameter sets). Some resources are output resources of some process and in the same time input resources for some other. We are calling those “transactional” resources. An images plate, for example, is the output resource of the process “image setting” and in the same time an input resource of the “printing” process. A physical press would be an example for a non-transactional input resource of the printing process. Note, that the transactional resources imply the sequence of processes. Thus, they are important for scheduling.

In summary, we would like to justify our motivation for a design a workflow puzzle that on the one hand, we consider the integration of technical processes in print production extremely important for the graphical industry and on the other hand, we see that students have a certain lack of knowledge with this respect. Getting an overview of production sequences is the first right step in this direction.

Our puzzle game is based on the process-resource model. The player can lay down puzzle pieces that represent either processes or resources. Such a puzzle pieces is also called a “card” in this paper and in the code of our game. Since in a real production environment the model can get complicated with dozens of processes and hundreds of resources, we had to simplify the model. We archived that by focusing on transactional resources.

We need to clarify that the names of the processes and the resources that we are using in the game, are not necessarily the names that CIP4 specified in the JDF specification. The latter are frequently some-

what abstract (like “RunList” or “Component”) and a bit hard to comprehend for students. We also like to mention, that the process-resource model is not limited to a model for print production only, but suits any workflow. This holds for our puzzle as well.

We believe that this re-design of the analogue card game to an online puzzle game has several advantages for the students:

- They have access to online-help about processes and resources if they need more information about them
- Since they do not need a physical card game, they can play the puzzle outside the class
- They get an immediate respond if the lay the card in a wrong order

## How to play the puzzle

We hosted the puzzle game under:

<https://www.ryerson.ca/~wdp/workflow-game/>

We encourage you to try it yourself.

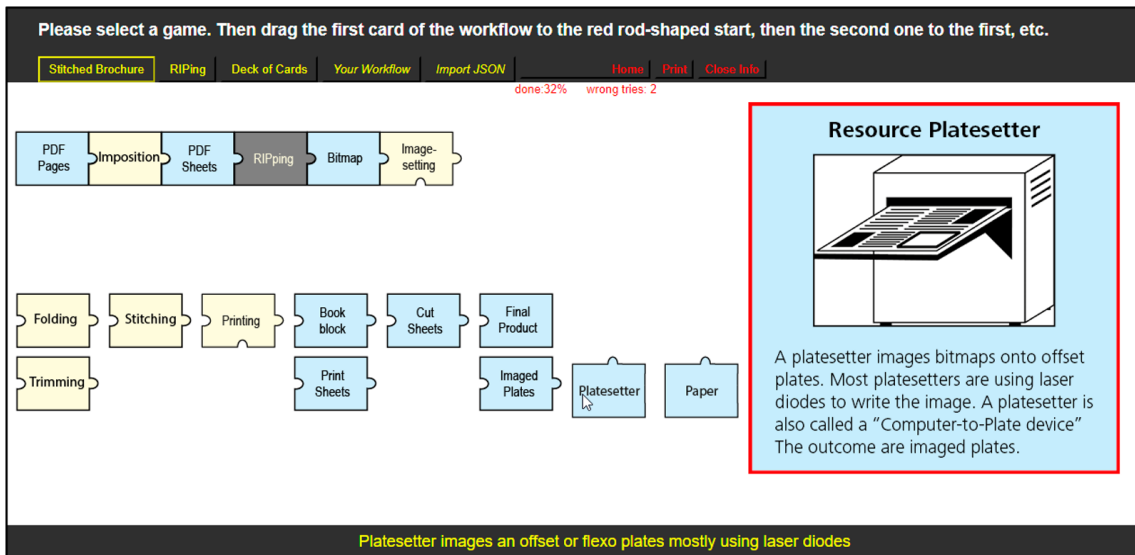
With the puzzle, we are pursuing two different didactic goals. In the first case, we like to teach the sequence of different tasks for a certain workflow. Here we marked the cards either by a number or by some other strong hint how to place the cards, e.g. by some color scheme. In the second case, we are asking the player to do his or her own research about the sequence of processes and resources. For that, there is information attached to each card. If the player hovers over a card, he or she will see a short statement at the footer about what the card represents in a yellow typeface. If that is not enough, a double click opens a window displaying a longer explanation in a pop up (framed in red color) giving some hints concerning the previous and next cards.

A counter counts the successful placements of cards as well as the number of failed attempts. We would consider this player best, who got the lowest number of wrong tries.

All yellow cards in Figure 1 represent processes, the gray one a group of processes (Interpreting, Rendering, and Screening) and all blue ones resources. The six card in the top row have already been moved to the correct position, the cards on the lower part have not. The small red information on the white background is saying that 32% of the cards are on the right position and two attempts for moving a card failed (because it was the wrong card).

The player receives some feedback when he or she lays out a card. If it is correct, a tone sounds and a textual confirmation comes up. If the card is





» **Figure 1:** Puzzle "Stitched brochure"

wrong, there is either a special indication of why the card is wrong or just a general objection.

Figure 2 shows another example of a puzzle game with a different card design. Here, only a small part of the overall production workflow is modeled, i.e. the RIPping process group.



» **Figure 2:** Puzzle RIPping

## Tools

We wrote the puzzle game in HTML 5 (W3C, 2017) and JavaScript (w3schools.com, 2020a). We deployed the JavaScript libraries jQuery version 3.5.1 and jQuery UI version 1.12.1 (The jQuery Foundation, 2020). Editing the code, we used Brackets 1.14 (Adobe, 2020). For testing and debugging the HTML and JavaScript, we loaded the code into Google Chrome (Version 83.0.4103.61) and Mozilla Firefox (version 76.0.1). As a web server is necessary for the test, we installed XAMPP, version 7.4.6 for Windows, (Apache Friends, 2020) locally, in particular the Apache HTTP Server. All of these tools can be downloaded free of charge.

## Implementation

We defined a class Card to store the relevant data for each card like the file name, the dimensions, the

neighboring cards and the HTML object (see Figure 3). The data we either defined directly in the script, e.g.

```
c301= new Card('card301','card301.png',
93,61,'card302',null,null'text info');
```

or by an import of a JSON file. For the specification of this data interchange format see (ECMA, 2017), for an easy online learning (w3schools.com, 2020b). Figure 4 shows an excerpt of our JSON file. The import works via HTTP. The jQuery method getJSON() reads the JSON data into the script. The so-called response function results in (key,value) tuples that need to be mapped to all Card object. Please note that the method getJSON() normally runs in the background (*asynchronous*), i.e. it take a while until the data is read in. Since the script should not continue in our case, before all data is available (otherwise we get many *undefined* errors), we need to switch to the synchronous modus beforehand by

```
$.ajaxSetup({ async: false});
```

Ajax is an acronym for Asynchronous JavaScript and XML.

For each Card object, we are creating dynamically an HTML element <div>. Using the jQuery function addClass() and innerHTML, we can complete the element by defining a class for it as well as the usual HTML sub-element <img> with property src specifying the path to the image file. These elements we have to append to the HTML Document Object Model (DOM) structure. Moreover, we added the HTML objects to the Card structure – see objectHTML in Figure 3. All Card objects of a game are pooled in an array that we called cardObjects. With this array, we have all necessary information for all cards ready to lay them down on the window.

For moving the cards is very easy to implement, because it is a given jQuery method called draggable.

```
class Card {
  constructor(id, scr, width,height,
    neighRight,neighBottom,neighLeft
    info,objectHTML){
    this.id =id;
    this.scr=scr;
    this.width=width;
    this.height=height;
    this.neighRight=neighRight;
    this.neighBottom=neighBottom;
    this.neighLeft=neighLeft;
    this.info = info;
    this.objectHTML = objectHTML;
  }
  ...
}
```

» **Figure 3:** Class Card hold information for each card

```
[
  {
    "id":"card201",
    "scr":"card201.png",
    "width":93,
    "height":61,
    "neighRight":"card202",
    "neighBottom":"null",
    "neighLeft":"null",
    "helpText":"Create cards using a
      graphic editor"
  },
  ...
]
```

» **Figure 4:** JSON data of a Card object

A card is supposed to snap to the correct position if it is close to its predecessor card, which in turn has been put down already correctly to the process/resource structure. To archive that, we have to check two things

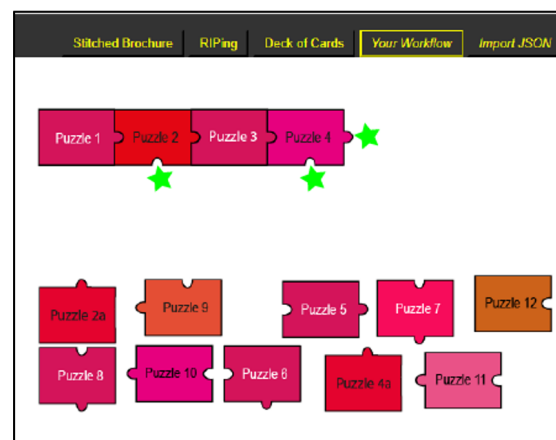
- i. Is the card close to a card, which needs a neighbor?
- ii. Is it the correct card in the process/resource chain?

For evaluating situation in i) we defined “hotspots”. A hotspot is an (x, y) position to which another card can be placed. Figure 5 shows the constructor of our class hotspot. Since our workflows need not to be strictly linear but rather allow ramifications, we might have several hotspots in the same time. In Figure 6, we marked each hotspot with a green asterisk. Therefor we defined an array of hotspot objects. Each card, which the player drags to some place, has be checked if it is close to one of those hotspots. In each hotSpot, information is stored, which is the correct neighbor. The trickiest part of the script, however, is the positioning of the card.

Depending if the predecessor card has an output “knob” or not, the card must me positioned differently. There are more situations like that which needs extra care.

```
class hotSpot{
  constructor(x,y,nextCardRight,
    nextCardBottom, nextCardLeft
  {
    this.x = x;
    this.y = y;
    this.nextCardRight = nextCardRight;
    this.nextCardBottom= nextCardBottom;
    this.nextCardLeft = nextCardLeft;
  }
  ...
}
```

» **Figure 5:** Constructor of the class hotSpot



» **Figure 6:** Each hotspot is marked with an asterisk

## Conclusion

The Online Workflow Puzzle illustrates the trends toward “gamification” and asynchronous learning in the online environment. Details on this topic can be found in (Kim et al., 2018). As compared with the original printed “card deck,” the online version enables a wider audience of graphic arts students to explore various workflow steps and understand the connection between them. The configurable nature of the puzzle enables it to evolve with new technologies and the workflows in which they are used.

Many details are still missing in this puzzle game, like a

- cards with more than one inter-faces for output resources,
- support for more than one starting point,
- processing more than one JSON file with an automatic extension of workflow choice in the UI when importing new JSON data.

Finally, the game could have a completely different architecture in order to support “arbitrary” work-flows and not just predefined ones. That is, the front end (web browser) could have access to a superset of cards in unlimited numbers. The cards are dynamically generated by the software according to the player’s choice of inputs and outputs for all four edges. The production configuration, which the player constructs, is sent to a backend software for evaluation. The backend software works with a knowledge base, consisting of rules that can be edited independently. This way, configurations that contradict one or more rules (as the printing process is followed by the imposition process) could be detected and warning could be forwarded to the frontend and ultimately to the player.

Kim, S., Song, K., Lockee, B. & Burton, J. (2018) Gamification in Learning and Education. Cham, Springer. Available from: doi: 10.1007/978-3-319-47283-6

The jQuery Foundation (2020) jQuery 3.5.1. Available from: <https://jquery.com/> [Accessed 28th August 2020].

W3C (2017) HTML 5.2. Available from: <https://www.w3.org/TR/html52/> [Accessed 28th August 2020].

w3schools.com (2020a) JavaScript Tutorial. Available from: <https://www.w3schools.com/js/DEFAULT.asp> [Accessed 28th August 2020].

w3schools.com (2020b) JSON – Introduction. Available from: [https://www.w3schools.com/js/js\\_json\\_intro.asp](https://www.w3schools.com/js/js_json_intro.asp) [Accessed 28th August 2020].

## References

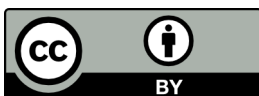
Adobe (2020) Brackets. Available from: <http://brackets.io/> [Accessed 28th August 2020].

Apache Friends (2020) XAMPP. Available from: <https://www.apachefriends.org/de/index.html> [Accessed 28th August 2020].

CIP4 (2020a) JDF Specification 1.7 final. Available from: <https://confluence.cip4.org/display/PUB/JDF> [Accessed 28th August 2020].

CIP4 (2020b) XJDF 2.1 final. Available from: <https://confluence.cip4.org/display/PUB/XJDF> [Accessed 28th August 2020].

ECMA (2017) The JSON Data Interchange Syntax. 2nd ed. Geneva, ECMA International. Available from: <https://www.ecma-international.org/publications/files/ECMA-ST/ECMA-404.pdf> [Accessed 28th August 2020].



© 2021 Authors. Published by the University of Novi Sad, Faculty of Technical Sciences, Department of Graphic Engineering and Design. This article is an open access article distributed under the terms and conditions of the Creative Commons Attribution license 3.0 Serbia (<http://creativecommons.org/licenses/by/3.0/rs/>).



# An investigation on skeleton-based top-down modelling approaches of complex industrial product

## ABSTRACT

*In industry, today's approach to assembly design is still largely based on a bottom-up approach which, in contrast with the most advanced top-down techniques, is unfit to deal with very large and complex products. The reason for this lies in the high number of relationships to be established between parts and in the lack of a high-level control of the assembly design. This makes the management of design changes a labor-intensive process and the capture of design intent difficult to achieve. The paper, referring to the most advanced research fields of Concurrent Engineering and Knowledge-Based Engineering, focuses on a top-down modelling approach based on skeleton, which constitutes the most natural but still scarcely exploited way to attain a high reactivity to design modifications. Through the application of suitable methodologies, such as that one for a SKeLeton geometry-based Assembly Context Definition (SKL-ACD), the skeleton is also able to capture and codify assembly process engineering information since the early phases of the product development process. With the purpose of promoting the knowledge of these skeleton-based modelling techniques, that have a great relevance for training professional, technical and mechanical engineers, this paper implements the SKL-ACD methodology to an industrial case study in order to identify, with a unique and repeatable workflow, the reference geometrical entities and the mutual relationships to embed into the product skeleton. The skeleton types and the related fields of use are also described, placing particular emphasis on problems or shortcomings still not resolved, especially in consideration of the need to assist the designer in defining the impact of a parameter on assembly modification and in avoiding loops while defining formulas. A new tool, in the form of a multilayer graph, is finally proposed that is able to display and differentiate clearly the formulas, the design parameters and the impact of their modification on skeleton entities and members of the assembly.*

## KEY WORDS

Knowledge-Based Engineering, Top-Down Assembly Design, Skeleton, Product Parametrization

Claudio Ciacchioli   
Anna Eva Morabito 

University of Salento, Department of  
Engineering for Innovation, Lecce, Italy

Corresponding author:

Anna Eva Morabito

e-mail: [annaeva.morabito@unisalento.it](mailto:annaeva.morabito@unisalento.it)

First received: 8.7.2020.

Revised: 27.8.2020.

Accepted: 7.9.2020.

## Introduction

The design process today is influenced by the need for better, less expensive, and faster-to-market products. This requires the implementation of innovative strategies capable of achieving and maintaining a consistently

high level of quality, both for the final product and for the entire development process. Many of these ones aim at making the early stages of this process more knowledge-intensive through the parallel execution of tasks and the implementation of a collaborative multidisciplinary decision-making process. These are the

---

basic premises for Concurrent Engineering (CE), i.e. a workflow where the phases of the product development process are no longer in rigid succession with each other, but run simultaneously. Thanks to this strategy, the early design process does not focus only on the basic functional aspects of the product but also on specific issues of downstream stages, such as design analysis, manufacturing simulation, assembly sequence planning, production, maintenance, disposal, etc. This allows concentrating the most of design modifications in the early phases of the development process, when they are cheaper and the product design is more flexible.

The traditional design approach is based on parametric and feature-based CAD models, which give a 3D digital representation of the product geometry enriched with technical and technological information and capable of capturing, if well parameterized, the design intent. These CAD models, however, cannot describe the design choices that led to a specific product configuration. Knowledge Based Engineering (KBE) is the design methodology that, by employing specific software tools, is capable to enrich the CAD model by embedding design rules and product and process engineering principles (for example manufacturing data, tooling data and structural information) in order to formalize the design rationale. In doing so, KBE allows capturing and systematically reusing product and process engineering knowledge. This is crucial for reducing design time and costs, automating repetitive operations and being supportive for conceptual design (Rocca, 2012; Chandrasegaran et al., 2013). The knowledge capture or acquisition is a critical phase for KBE diffusion, especially when dealing with conceptual design problems. These problems are usually wicked or ill defined (i.e. incomplete and contradictory) and with changing requirements that are often difficult to recognize. FBS (Function-Behavior-Structure) Ontology is the most promising and widespread solving approach, which categorizes the properties of a product to design or to innovate into three levels: function (“what the object is for”), behavior (“what the object does”) and structure (“what the object consists of”) (Gero & Kannengiesser, 2014).

Parallel execution of tasks and cooperation between teams also require the adoption of a top-down product design approach, which begins by defining the product structure before detailing its individual parts (Vielhaber et al., 2004). Thanks to this approach, a product vision, which can be enriched with engineering knowledge, is available from the earliest stages of the development process.

Observing from a more closely CAD perspective, the top-down design paradigm can be very efficiently implemented by a skeleton-based assembly modeling approach. The skeleton is a control structure containing the reference geometry that will drive the key dimensions and positions of the components of the

assembly, together with the relative space allocations. This allows efficiently managing the scalability and responsiveness of the product to the propagation of changes made in accordance with the design intent.

The skeleton is also potentially able to represent the knowledge of the product coming from downstream stages of the development process. Recently, various methodologies have been proposed that, starting from data on assembly sequence planning or manufacturing process, compute and define automatically the geometry of product skeleton. Among these, the methodology for Skeleton geometry-based Assembly Context Definition (SKL-ACD) aims at integrating assembly process engineering knowledge in the early phases of the product development process (Demoly et al., 2011). This methodology, which differs significantly from the traditional one where the assembly sequence is defined after the detailed design phase, improves the productivity and efficiency of the design by reducing the iterations due to the definition of poor assembly requirements. A CAD model of the industrial product, suitably parameterized, knowledge-based and capable of acting as master model for a family of products can be, therefore, obtained reducing both repetitive tasks for the designer and time to market for the company.

In order to promote the use of skeleton-based modeling techniques able to integrate the knowledge coming from the downstream phases of the development process, this paper first describes the main steps of the SKL-ACD methodology through the implementation of a simple case study that allows students to understand the design issues involved. The application of SKL-ACD methodology allows identifying the reference geometry to be incorporated into the skeleton. Current CAD systems offer different types of skeleton. This paper describes them by underlining the related fields of use and placing particular emphasis on open issues or shortcomings still not resolved, especially in consideration of the need to assist the designer in defining the impact of a parameter on product design and in avoiding loops while defining formulas.

Particularly, a problem still addressed unsatisfactorily by current CAD systems, concerns the availability of tools capable of visualizing and managing efficiently the product parametrization so that design modifications propagate in agreement with the design intent. The designer, in fact, chooses a set of parameters to guide the skeleton and quickly change some key variables (such as dimensions, positions and space allocations) of the assembly members. Since these modifications are propagated, through the skeleton, to the parts or sub-assemblies downstream, the designer should be always aware of which members are affected by a specific parameter. In order to navigate this domain of relations, CAD software currently implement a set

of tools, which, as will be shown by this paper, are not always able to support adequately the designer activities. After having given an overview of these tools, the paper proposes the construction of a multilayer graph, as a new way to visualize and manage effectively the paths through which the parameters of the skeleton influence the product geometry. In the case of a top-down design approach, such as the skeleton-based one for which the reuse of parameters makes the tracing of the related paths more complex, this issue is actually more felt.

The paper has the following outline. Section 2 surveys, from a CAD perspective, the concept of product skeleton pointing out the basic principles for a top-down modelling approach based on skeleton. Section 3 describes synthetically the case study for which the steps of the SKL-ACD methodology, used to identify the skeleton's reference geometry, are then explained. Section 4 overviews the main skeleton types and the related fields of use. Particular emphasis is placed on the tools currently implemented to visualize and manage the paths of skeleton parameters and formulas. Various aspects of the issues addressed are highlighted and discussed in section 5, where a multilayer graph is proposed as a new visualization tool to better support the designer when tracking parameters paths. Finally, conclusions are provided in section 6.

## Skeleton-based modelling approach

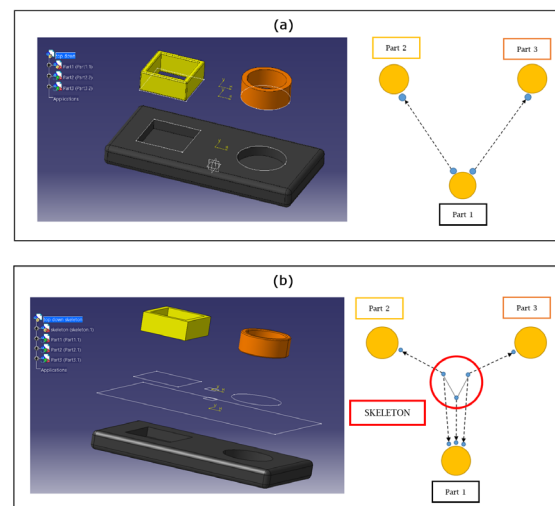
The implementation of a collaborative and simultaneous design approach leads, from a CAD perspective, to the modification of the assembly design paradigm from bottom-up to top-down (Vielhaber et al., 2004). In conventional top-down approach, the parts are modelled in the context of the assembly referencing the geometry of existing components, i.e. creating external references pointing to existing geometry in the assembly. Any geometrical element (sketch, point, line, curve, surface, etc.) defined in a component can be reused to model and to control another part, referred to as contextual part. When designing with this approach (often also referred to as “design in context”), the contextual part is automatically updated as soon as the geometry of the referenced component changes. A contextual link between the driving (or referenced) component and the driven (or contextual) component is then established.

Figure 1(a) simply illustrates this approach through the example of a product made of three blocks, shown in exploded view for clarity. The yellow and orange parts (respectively called Part 2 and Part 3 in the graph reported on the right side of Figure 1(a)) have been modelled in the context of the assembly from the sketches obtained by projecting respectively the two edge loops

delimiting the Part 1's pockets. An equivalent result can be obtained by copying associatively the sketches of these pockets respectively into Part 2 and Part 3. In doing so, *contextual links* are established between Part 1 and Part 2, and Part 1 and Part 3 (as shown by arcs of the graph reported on the right side of Figure 1(a)). Therefore, any change on pockets' sketches of Part 1 is automatically propagated to the other parts.

In the conventional top-down approach, additionally, a component's parameter can be reused in another part to connect the related geometries. This occurs through the creation of *relations* (i.e. formulas), by which any change made to the referenced parameter will be reflected in the others by modifying the related geometries.

The skeleton-based approach identifies a specific way to define relationships between parts by centralizing them on the skeleton itself. Figure 1(b) shows the implementation of this approach to the plain example of the three blocks. The skeleton is composed of three sketches and each of them is either directly referenced during the geometric modelling of the related part or associatively copied inside this one. In this last case, an external reference is created within each part well before detailing the corresponding geometric model. Consistently, the arcs of the graph of Figure 1(b) represent the contextual links between skeleton and parts of the assembly. Any change in the skeleton's sketches will propagate to the other contextual parts by modifying the related geometries.



» **Figure 1:** Top-down modelling approaches: conventional (a) and with skeleton (b)

Skeleton geometry can also be used to position the components of the product through the selection of a suitable set of assembly constraints that establish *positional links* between the skeleton and the components of the product. In order to capture the design intent, skeleton parameters can be created and then referenced by the assembly members

through the definition of formulas. The assembly members reuse, therefore, the skeleton's elements to define the related underlying design framework.

Any change to the overall design can be made on the skeleton model and, by means of the before-mentioned relationships (i.e. contextual, positional and by formulas), is automatically propagated to the driven components. This allows an improved management of high-level design modifications. As the components are not directly linked to each other, the deletion of a component within an assembly will not affect the others. Moreover, since the skeleton model does not use external references within the assembly to define its geometry, the issue related to the circular references is avoided. All external references, in fact, only point to the skeleton model so that the direction of information is always downwards, from the skeleton model to the other components and the relationships cannot interfere with each other. Another advantage of this approach is that the components can be edited separately making tasks parallelization and cooperation possible between different professional figures. Thanks to the afore-mentioned relationships between skeleton and components, in fact, the designer can be sure that design data is up to date.

The skeleton-based approach may be also useful to address issues related to the protection of intellectual property. When designing a product, companies usually make use of third-party components. In these circumstances, the intellectual property of a participating company should be protected from the others. This safeguard should not be an obstacle to product design collaboration. Moreover, each enterprise usually utilizes a different CAD software, which represents a further obstacle for collaboration and designers often rely on ISO 10303 STEP as interchange file format that however is not parametric by nature. Skeleton design can address these issues by becoming a neutral reference model (Mun, Hwang & Han, 2009): each company involved in product design can work on the reference geometry of the skeleton, which does not contain any detailed description of the parts, but only the information necessary to meet the requirements of the other collaborating companies.

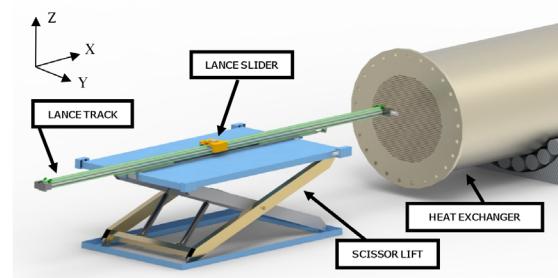
## The SKL-ACD methodology

Industrial plants generally employ heat exchangers of different sizes so that the application of a skeleton-based CAD approach to the design of a pipe bundle cleaner can be beneficial for scalability purposes. A pipe bundle cleaner is an automatic device, designed for cleaning heat exchangers and other kinds of equipment that experience fouling: it consists of three main functional groups, namely a scissor lift, a lance track and a lance slider. The machine operates introducing sequentially into each tube of the exchanger a rigid lance with a high-pressure nozzle threaded on one end.

At the other end, high-pressure water is pumped (up to 3000 bar) with flows that reach hundreds of liters per minute; thus, the hydrodynamic action removes deposited materials that previously choked the tubes.

The tube bundle appears as a matrix of thousands of holes that can reach 2 meters in diameter; the tube length varies upon the size of the heat exchanger, usually from 6 to 11 meters.

In reference to the coordinate system in Figure 2, the scissor lift is responsible for the movement along the Z-axis. The rigid lances lay on the lance track, which can slide along the scissor lift table on the Y-axis by a chain transmission. The combination of Z and Y translations guarantees the correct positioning of the lances with respect to the holes matrix. The lance slider, where the hydrodynamic connections with the lances occur, can slide along the X-axis via another chain transmission, introducing the lances into the heat exchanger and beginning the cleaning process.



» **Figure 2:** *Rendering of the cleaning process*

The SKL-ACD methodology allows defining the skeleton's reference geometry consistently with the product structure and the assembly sequence planning engineering information (Demoly et al., 2011). The product structure is identified starting from existing design concepts or Bill Of Materials (BOM) of similar previous designs retrieved from the company know-how. Table 1 shows the 15 parts or groups of parts which make up the product structure for the case study considered.

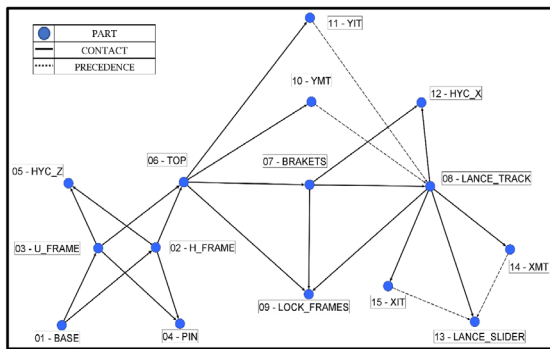
Starting from the assembly sequence of the product, the part-to-part relational information on physical contacts and precedence constraints are embedded in a directed graph and in the related adjacency matrix. Each vertex of the directed graph is a part or sub-assembly, while each edge identifies a relationship between vertices. In the directed graph for the pipe bundle cleaner of Figure 3, the vertices are the parts or the groups from Table 1. The precedence constraints are represented by a dotted line and apply to the chain transmissions of both lance track (part 8 of BOM of Table 1) and lance slider (part 13 of Table 1). These transmissions, in fact, need to be mounted after the other components are in place for interference reasons.



**Table 1**

BOM for the pipe bundle cleaner

Num.	Name
01	BASE
02	H_FRAME
03	U_FRAME
04	PIN
05	HYC_Z
06	TOP
07	BRACKETS
08	LANCE_TRACK
09	LOCK_FRAME
10	YMT
11	YIT
12	HYC_X
13	LANCE_SLIDER
14	XMT
15	XIT



» **Figure 3:** Directed graph for the pipe bundle cleaner

Figure 4 represents the adjacency matrix for the case study.

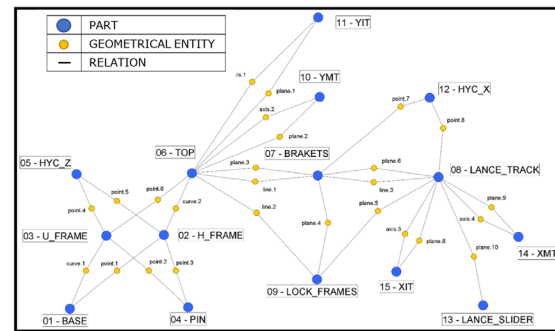
	01	02	03	04	05	06	07	08	09	10	11	12	13	14	15
01	0	1	1	0	0	0	0	0	0	0	0	0	0	0	0
02	-1	0	0	1	1	1	0	0	0	0	0	0	0	0	0
03	-1	0	0	1	1	1	0	0	0	0	0	0	0	0	0
04	0	-1	-1	0	0	0	0	0	0	0	0	0	0	0	0
05	0	-1	-1	0	0	0	0	0	0	0	0	0	0	0	0
06	0	-1	-1	0	0	0	1	0	1	1	1	0	0	0	0
07	0	0	0	0	0	-1	0	1	1	0	0	1	0	0	0
08	0	0	0	0	0	0	-1	0	1	-λ	-λ	1	1	1	1
09	0	0	0	0	0	-1	-1	-1	0	0	0	0	0	0	0
10	0	0	0	0	0	-1	0	λ	0	0	0	0	0	0	0
11	0	0	0	0	0	-1	0	λ	0	0	0	0	0	0	0
12	0	0	0	0	0	0	-1	-1	0	0	0	0	0	0	0
13	0	0	0	0	0	0	0	-1	0	0	0	0	0	-λ	-λ
14	0	0	0	0	0	0	0	-1	0	0	0	0	λ	0	0
15	0	0	0	0	0	0	0	-1	0	0	0	0	λ	0	0

» **Figure 4:** Adjacency matrix for the pipe bundle cleaner

The numbers populating this matrix have a sign that reflects the directionality of the part-to-part relation,

namely the verse of the arrow for the generic edge of the directed graph. The element  $a_{ij}$  of this matrix is +1 or +λ if it represents respectively a contact or precedence relation that starts from the part associated to the  $i^{th}$ -row and leads to the part corresponding to the  $j^{th}$ -column. Conversely, it is -1 or -λ if describes respectively a relation starting from the part of the  $j^{th}$ -column and leading to the part of the  $i^{th}$ -row.

Each edge of the directed graph also identifies a potential kinematic/technological pair (or joint), which can be of different kind based on the relative degrees of freedom (DOF) allowed by the part-to part relative motion. Assembly constraints and skeleton geometric entities can be generated, therefore, for each type of joint by means of an appropriate codification (e.g. a revolute joint is defined by the pairs line-line and plane-plane). Figure 5 shows the results of this step for the pipe bundle cleaner.



» **Figure 5:** Skeleton entities definition

Based on the 13 constraints described in the Technologically and Topologically Related Surfaces (TTRS) theory (Desrochers & Clément, 1994), new constraints between the skeleton entities can be then defined. A new graph, called “skeleton graph”, is therefore built based on these geometric entities and mutual relationships. Figure 6 shows the “skeleton graph” for the pipe bundle cleaner.

The geometric model of the skeleton emerges from this graph through the CAD modelling of the aforementioned geometric entities and of the mutual geometric relationships. Consistently with these data, the skeleton incorporates also a set of parameters so that the CAD model of the pipe bundle cleaner is able of acting as master model for a whole family of products, reducing both repetitive tasks for the designer and time to market for the company.

Table 2 shows the 15 skeleton parameters able to drive the pipe bundle cleaner geometry and the relative variability ranges. Among these, 11 parameters (in red) have been identified in order to drive the variability of product dimensions. The other 4 (in green), directly related to geometrical relations between the skeleton entities, are kinematic parameters representing the actual degrees of freedom (DOF) of the machine.

## CAD techniques for skeleton-based modelling approach

Three are the main modelling techniques aimed at generating as many skeleton typologies; they are named respectively:

- Static skeleton
- Kinematic skeleton
- Knowledge-driven skeleton

This paper focuses on the first two types, which have an immediate application on the designer's activities, although they are still underutilized particularly by small and medium-sized companies. The techniques for modelling knowledge-driven skeletons, on the other hand, need to be contextualized in a company framework for the necessary knowledge acquisition and require object-oriented programming to formalize know-how.

The static skeleton is described by a single part able to drive the assembly geometry and it is useful to the top-down design of assemblies for which one does not deem necessary to perform a detailed kinematic analysis.

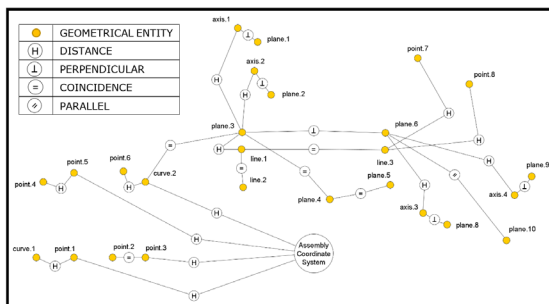
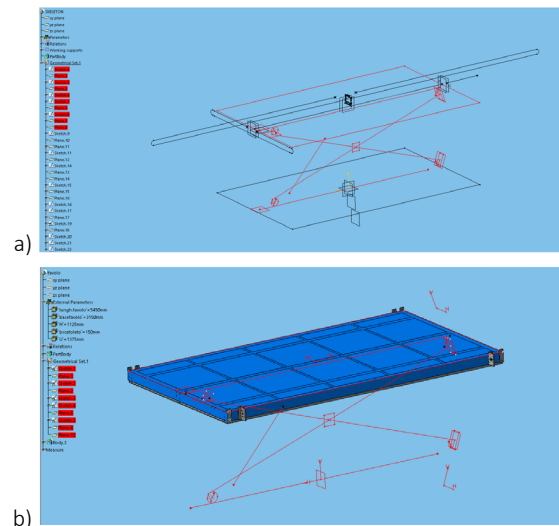


Figure 6: Skeleton graph

Referring to the case study under examination, Figure 7(a) shows the static skeleton modelled within CATIA V5. This is constructed as a part containing the reference geometrical entities and the mutual relationships shown in the graph of Figure 6. During the modelling of a member of the assembly, these entities are referenced by direct selection or copied associatively. Figure 7(a) also illustrates in red the reference geometrical entities required by the TOP (i.e. part 6 of the BOM in table 1), which is shown in Figure 7(b).



» Figure 7: Static Skeleton modelled in CATIA V5 for the case study (a). The TOP part of the case study with the skeleton entities "pasted with link"

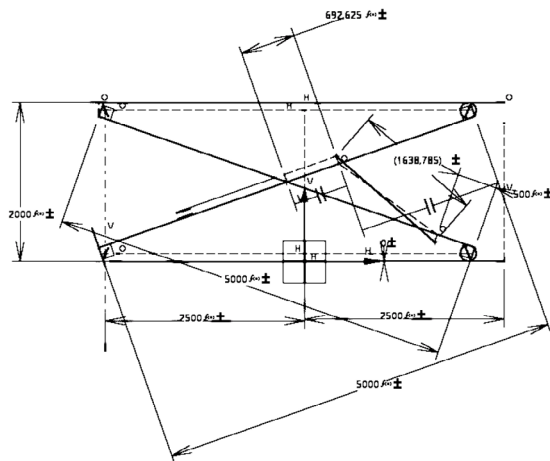
This way of "fixing" each part to a common static frame (i.e. the static skeleton) allows investigating only instantaneous product configurations. In other terms, by varying the kinematic parameters of the static skeleton in the constraints respect (such as those of the sketch

Table 2

Skeleton parameters for the pipe bundle cleaner

Num.	Code	Range/Formula [mm]	Description
01	B	3000 – 5000	Scissor length
02	BS	100 – 150	Hollow section base
03	HS	200 – 300	Hollow section height
04	H	BT/4	H frame span
05	U	H + 250	U frame span
06	SH	150- 200	Square hollow section
07	HT	600- 3600	Table height (z)
08	BT	3150- 3500	Table base
09	LT	B + 300	Table length
10	TY	-1300- 1300	Lance track translation (y)
11	LB	3650- 5650	Lance track length
12	TX	0 – 500	Lance translation (x)
13	TC	-5650- 5650	Lance slider translation (x)
14	S	5- 8	Hollow section thickness
15	C	$(0.02805 * B^{**2} + 0.08045 * B) - 0.18$	Cylinders arm

of Figure 8 belonging to the case study's skeleton), it is possible to visualize the kinematic behaviour of the product. This model, however, remains a substantially rigid structure that does not allow to answer any query about the relative motion between the parts (such as to determine the direction of motion of the assembled parts with respect to other parts or to find the velocity and acceleration of any point on any part during the motion of the mechanism).



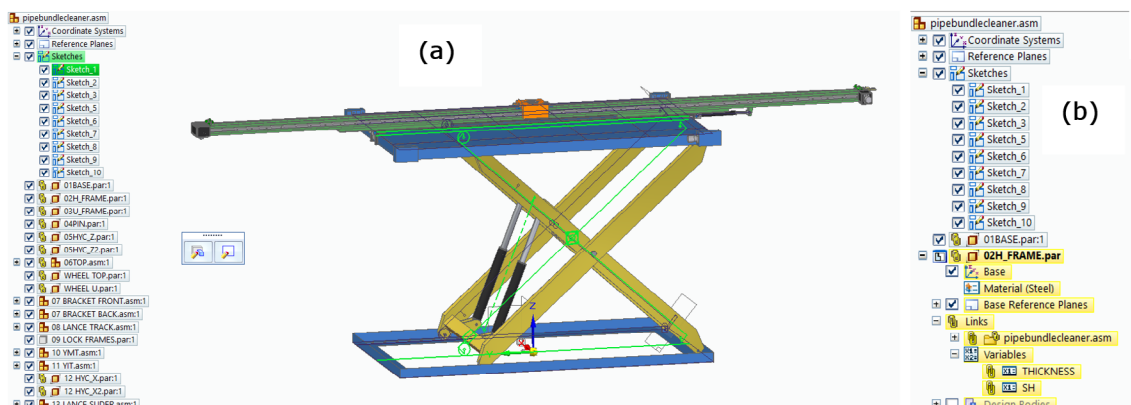
» **Figure 8:** 2D constraints embedded in a sketch of the static skeleton constructed within CATIA V5 for the case study

The kinematic skeleton is modelled as an assembly consisting of parts, each containing only the geometric entities that will be referenced by the related member of the assembly. Within CATIA, for example, the construction of this type of skeleton takes place with a technique that actually overturns the classic bottom-up use of software modules exemplified by the workflow sequence: Part Design -> Assembly Design -> Digital MockUp (DMU) kinematics. In this case, perfectly in line with a top-down methodology, the user has to switch to the kinematic module to define the joints and the fixed part in order to create a mechanism from the skeleton

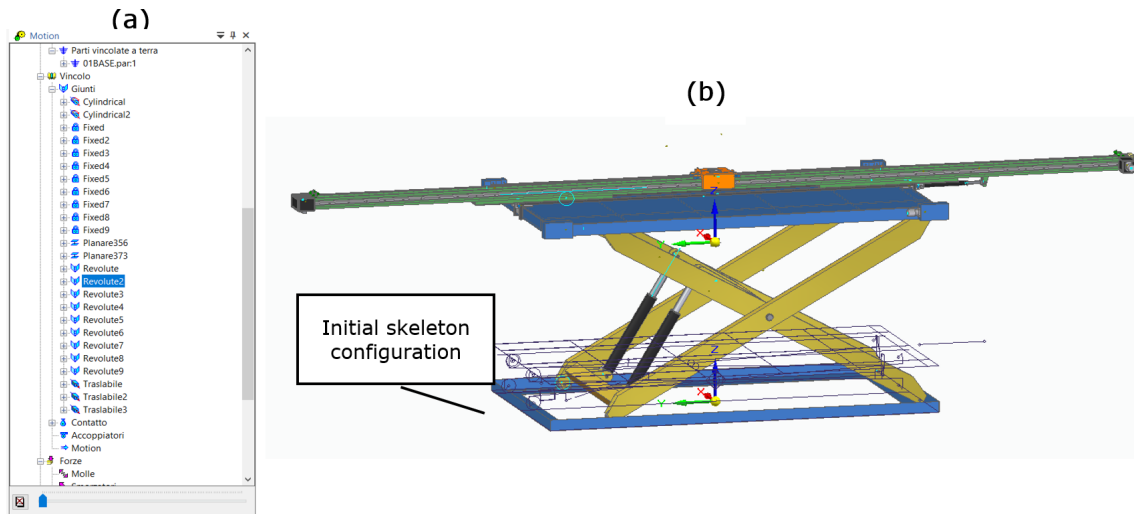
parts. By so doing, the software automatically defines also the minimal number of necessary assembly constraints. Then, the actual geometry of the parts is defined referencing directly the underlying skeleton geometry. Finally, each part is linked with its own skeletal part through the command called “Mechanism Dress up”.

Currently there are CAD systems (e.g. CREO) which have built-in features specifically devoted to skeleton modelling and available since the early steps of the product design. In other cases, as in CATIA V5, the distinction between static and kinematic skeleton is only procedural, so that it may be very difficult to switch typology when the assembly design is in an advanced state. Additionally, there are systems where the distinction between static and kinematic skeleton is useless. SOLID EDGE, for example, contrary to CATIA V5 allows the creation of 2D reference geometry (sketches, planes, etc.) directly at the product level. In other words, the assembly is not merely a set of parts and relationships, but it may contain its own geometry, which can be selected and referenced by lower level members through a projection operation. Thus, the assembly level constitutes a natural place to define skeletons, parameters and links. Figure 9(a) shows the pipe bundle cleaner assembly, constructed from reference datums and sketches defined at the assembly level. If some reference geometry is projected downstream while designing a part, a “links” node is created into the assembly tree, as shown in Figure 9(b), which constitutes the associative reference set for that specific part. Moreover, a “variables” node is also generated which includes the published parameters in use from the upper assembly level.

As for the workflow within SOLID EDGE, the Motion analysis module (devoted to the kinematic analysis of the mechanism) does not require the implementation of a specific type of skeleton, making the distinction between static and kinematic skeleton useless. Consequently, a skeleton can be designed by using the reference geometry that drives simultaneously several parts or



» **Figure 9:** The pipe bundle cleaner and the related skeleton (highlighted in green) constructed within SOLIDEDGE (a). The links node and the variables node for O2H\_Frame part (i.e. part O2 in the BOM of Table 1) (b)



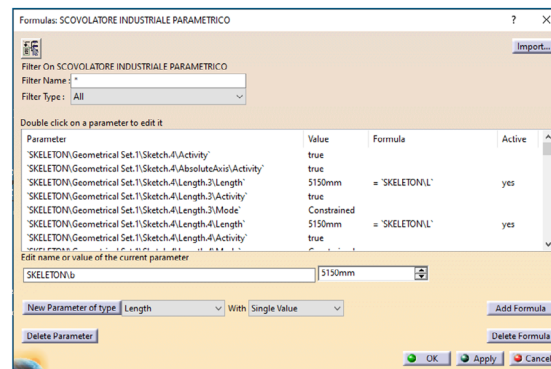
» **Figure 10:** Motion tree (a) and Motion simulation with skeleton as initial configuration (b)

part-by-part and then stored in a specific sub-assembly. The motion analysis will still act as a different scenario where functional simulation groups can be defined independently of how the product tree is hierarchically organized. Figure 10(a), for example, shows a motion tree for the case study that is different from the product tree. The skeleton can be used as a reference for an initial kinematic configuration but the joints defined in the motion environment are independent from the constraints defined between skeleton and parts. Consequently, while defining motion constraints, e.g. a curve on curve joint, skeleton geometry cannot be used and it is necessary to model the single parts first and then project those 3D features needed for joints definition. In Figure 10(b), the motion analysis of the lifting platform has been carried out, starting from the lower position defined by the initial skeleton configuration.

## CAD tools for visualization and management of product parametrization

The dimensional and kinematic parameters listed in Table 2 are created and embedded into the skeleton geometry through the definition of formulas (or relations). In order to drive the product geometry, linked copies of these parameters are created in the corresponding parts, where they are usually listed under the node of the external parameters. Although only 11 parameters were required to guide the scalability of the case study (i.e. to make the scissor lift and lance track scalable to various sizes of heat exchangers), the number of relations to be defined is rather high. For this reason, it is important that CAD systems include some tools for the tracking of information flows in the parameter network of the assembly. Many software, such as CATIA and SOLID EDGE, use a table or entry list for defining, visualizing

and managing formulas and parameters. Figure 11 shows, for example, the table with filters offered by CATIA V5.



» **Figure 11:** The table with filters offered by CATIA V5 to describe the formulas

Similarly, the “Peer Variables” command in SOLID EDGE opens an interface (shown in Figure 12) where the relations of every part of the assembly can be inspected and grouped, for example based on the respective sketch where they have been defined. This interface, always organized in the form of a table lets the user define formulas, link parameters downstream, establish value ranges and create simple IF-THEN rules.

To manage and visualize the parameters of a product effectively, it may be advisable to create a GUI interface. Figure 13 shows an example of GUI implemented by a VBA macro in CATIA V5 for the case study under examination. This type of interface is useful for verifying the propagation of the modification and ensuring that the variation of the driving parameters in the relative ranges does not generate impossible geometries and/or interferences between the members of the assembly. Moreover, since a VBA macro runs in background, the product geometry regeneration is faster than a manual update in the CAD environment.

Struttura	Type	Name	Value	Units	Rule	Formula
Sketch_9						
Sketch_7						
Sketch_8						
Sketch_7						
V4290	Dim	V4290	150,00	mm	Formula	= BS
V5122	Dim	V5122	2,50	mm	Formula	= S/2
V5514	Dim	V5514	2,50	mm	Formula	= S/2
Sketch_10						
Assembly Ke...						
PMI						
User Variables						
B	Var	B	5000,00	mm		
DS	Var	DS	150,00	mm		
I15	Var	I15	301,00	mm		
H	Var	H	2150,00	mm	Formula	BT-1000
U	Var	U	2650,00	mm	Formula	H+500
SH	Var	SH	200,00	mm		
HI	Var	HI	8600,00	mm		
BT	Var	BT	3150,00	mm		
LT	Var	LT	5300,00	mm		
LB	Var	LB	9650,00	mm		
TX	Var	TX	0,00	mm		
TY	Var	TY	0,00	mm		
TC	Var	TC	0,00	mm		
S	Var	S	1,00	mm		
C	Var	C	923,50	mm	Formula	=(0,02805*(B/1000)^2+0,08045*(B/1000)-0,...
MidSurfac...	Var	MidSurface_4...	0,500		Limit	
MidSurfac...	Var	MidSurface_3...	0,500		Limit	

» **Figure 12:** The table generated by the “Peer Variables” command in SOLID EDGE

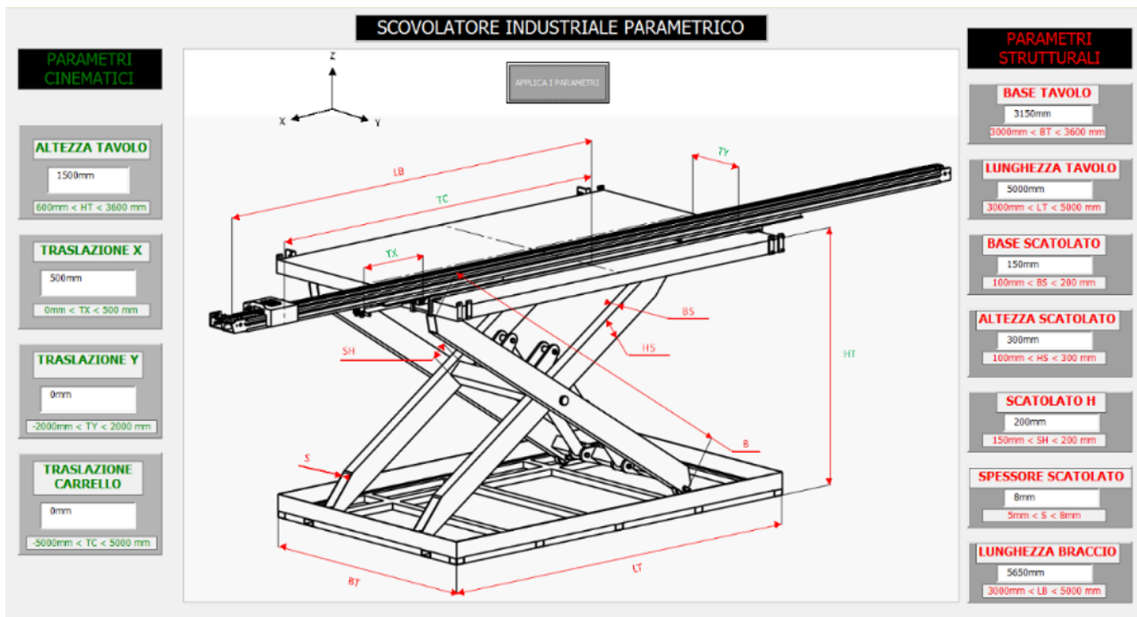
For a designer who needs to be supported in defining the impact of a parameter on modifying product geometry and in avoiding loops while defining formulas, the graph-based tools are more effective. Single-layer graphs, also filtered for considering only a certain type of relationships (i.e. positional, contextual and by formulas), can be generated within CAD systems such as CATIA V5 and CREO. The impact of the single parameter, on the other hand, can be investigated, by querying its parent-child relationships. However, these relationships are always limited to the context of the part under consideration. Not being able to visualize the complete path of the parameter, even if a contextual link exists downstream, is evidently a limit of the current CAD systems especially if

one considers that the parameter of a skeleton generally guides the dimensions of several parts of an assembly.

Recently, some researchers have addressed the problems of the documentation and visualization of complex networks of parametric-associative information within 3D CAD models, mostly proposing networks of planar relationships (Marchenko et al., 2011). However, an issue still exists concerning the development of effective visualization tools for supporting the designer in identifying and keeping track of parameters and formulas in a CAD product. This problem, as confirmed also by the investigation carried out here, is evidently even more critical in the case of a top-down design approach where the reuse of parameters makes the tracing of the related paths more complex.

Using the latest and most advanced tools of multilayer network visualization (McGee et al., 2019), such as Trix-picture of MuxViz, the product links, once extracted from the CAD database with a certain effort, can be rearranged spatially in a more effective way. Figure 14 shows a new type of graph, referred to as *Skeleton String Model (SSM)*, proposed here in order to display and manage more efficiently the CAD assembly parameters and formulas.

The SSM is a multilayer graph organized into two layers: the bottom layer is a graph very similar to that one shown in Figure 5, where the nodes are the parts/components of the product. An arc between two nodes is established when a skeleton entity is referenced by both the members associated with the two nodes respectively. Multiple arcs, therefore, may connect a given couple of nodes. The upper layer is a graph where the nodes represent the skeleton parameters. In the specific case



» **Figure 13:** An example of Product GUI Interface implemented by a VBA macro in CATIA V5 for the case study

of the pipe bundle cleaner these are 15 parameters differentiated into 11 dimensional parameters (red vertices) and 4 kinematic ones (green vertices). With the aim of pointing out the impact of the parameter modification on skeleton entities and assembly components, the SSM graph visualizes the relations (or formulas) as inter or intra-plane edges between nodes. An intra-plane relation on the upper layer shows a link between two or more parameters due to a given formula. Red and green inter-plane relations describe respectively the path of dimensional and kinematic parameters modification on assembly members and skeleton geometric entities impacted.










To highlight better these dependencies, the skeleton and components elements impacted inherit the color of the relation type, as shown in Figure 14. The application of the SSM to the case study points out, at first glance, a design intent focused on dimensional changes in the scissor lift (left part of the bottom layer) since the other components are designed to contain standard hydraulic accessories and thus they do not need to scale with the product.

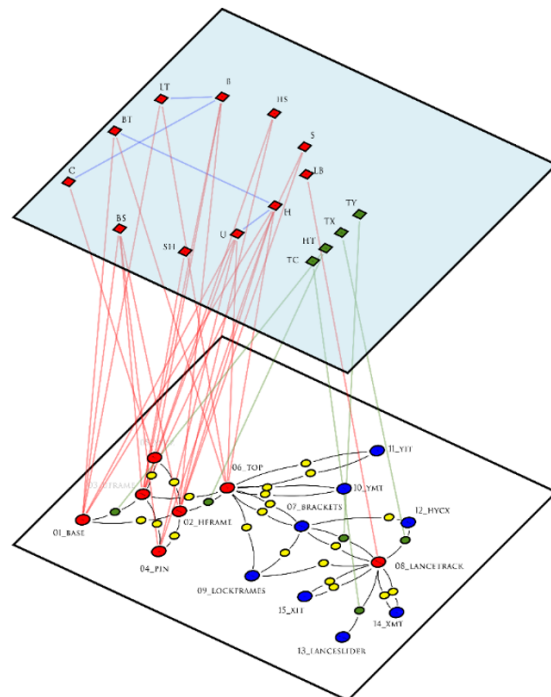
## Conclusion

The skeleton, i.e. a control structure able to drive the main positions, dimensions and space allocations of the members of complex products, allows to efficiently managing the scalability and responsiveness of the product to design modifications. Recently, new methodologies have shown that the engineering knowledge coming from

downstream stages of the product development process can be coded and embedded in the skeleton. The SKL-ACD approach, implemented here through a plain case study, allows identifying a skeleton graph starting from engineering information on assembly sequence planning. This graph includes the reference geometrical entities and the mutual relationships to be embedded in the related skeleton. This approach overturns the traditional methodology where the step for assembly sequence definition follows the design detailing phase, reducing the iterations due to the definition of poor assembly requirements.

With the purpose of promoting the knowledge of skeleton-based modelling techniques, that have a great relevance for training professional, technical and mechanical engineers this paper has described the different types of skeleton implemented and the related fields of use. Particular emphasis has been placed to the need of enriching the tools currently available for the display and the management of parameters paths. This is an important issue especially with a view to better support the designer when identifying and keeping track of the parameters involved by the several formulas defined in the CAD model of a complex product. A multilayer graph representation, the SSM graph, has been proposed here as an effective tool to visualize and differentiate, at first glance, the relations, the design parameters and the impact of their modification on skeleton entities and components of the assembly. This is useful especially in the case of a top-down design approach where the reuse of parameters makes the tracing of the related paths more complex.

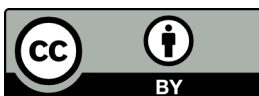
	PART
	IMPACTED PART
	DIMENSIONAL PARAMETER
	DIMENSIONAL RELATION
	SKELETON ENTITY
	IMPACTED SKELETON ENTITY
	KINEMATIC PARAMETER
	KINEMATIC RELATION
	PARAMETER RELATION



» **Figure 14:** *The Skeleton String Model graph (SSM graph)*

## References

- Chandrasegaran, S. K., Ramani, K., Sriram, R. D., Horváth, I., Bernard, A., Harik, R. F. & Gao, W. (2013) The evolution, challenges, and future of knowledge representation in product design systems. *Computer-Aided Design*. 45 (2), 204-228. Available from: doi: 10.1016/j.cad.2012.08.006
- Demoly, F., Toussaint, L., Eynard, B., Kiritsis, D. & Gomes, S. (2011) Geometric skeleton computation enabling concurrent product engineering and assembly sequence planning. *Computer-Aided Design*. 43 (12), 1654-1673. Available from: doi: 10.1016/j.cad.2011.09.006
- Desrochers, A. & Clément, A. (1994) A dimensioning and tolerancing assistance model for CAD/CAM systems. *The International Journal of Advanced Manufacturing Technology*. 9 (6), 352-361. Available from: doi: 10.1007/BF01748479
- Gero, J. S. & Kannengiesser, U. (2014) The function-behaviour-structure ontology of design. In: Chakrabarti, A. & Blessing, L.T.M. (eds). *An Anthology of Theories and Models of Design*. London, Springer, pp. 263-283.
- Marchenko, M., Behrens, B. A., Wrobel, G., Scheffler, R. & Pleßow, M. (2011) A New Method of Visualization and Documentation of Parametric Information of 3D CAD Models. *Computer-Aided Design and Applications*. 8 (3), 435-448. Available from: doi: 10.3722/cadaps.2011.435-448
- McGee, F., Ghoniem, M., Melançon, G., Otjacques, B. & Pinaud, B. (2019) The State of the Art in Multilayer Network Visualization. *Computer Graphics Forum*. 38 (6), 125-149. Available from: doi: 10.1111/cgf.13610
- Mun, D., Hwang, J. & Han, S. (2009) Protection of intellectual property based on a skeleton model in product design collaboration. *Computer-Aided Design*. 41 (9), 641-648. Available from: doi: 10.1016/j.cad.2009.04.007
- Rocca, G. L. (2012) Knowledge based engineering: Between AI and CAD. Review of a language-based technology to support engineering design. *Advanced Engineering Informatics*. 26 (2), 159-179. Available from: doi: 10.1016/j.aei.2012.02.002
- Vielhaber, M., Burr, H., Deubel, T., Christian W. & Haasis, S. (2004) Assembly-oriented Design in Automotive Engineering. In: Majranovic, D. (Ed.) *DS 32: Proceedings of DESIGN 2004, 8th INTERNATIONAL DESIGN CONFERENCE, DESIGN 2004, 18 – 21 May, Dubrovnik, Croatia*. pp. 539-546.








# Aiming for G7 Master Compliance through a Color Managed Digital Printing Workflow (CMDPW): Comparison of Compliance with Output Device Profile (ODP) vs. Device Link Profile (DLP)

## ABSTRACT

*The purpose of this applied research was to determine the influence of device link profile (DLP) in the color reproduction aimed at the G7 master compliance. The quality of digital color printing is determined by these influential factors: screening method applied, type of printing process, ink (dry-toner or liquid-toner), printer resolution and the substrate (paper). For this research, only the color printing attributes such as the G7 colors hue and chroma, gray balance, and overall color deviations were analyzed to examine the significant differences that exist between the two output profiles [Output Device Profile (ODP) vs Device Link Profile (DLP)]. These are the color attributes which are monitored and managed for quality accuracy during the printing. Printed colorimetry of each profile from the experiment was compared against G7 ColorSpace GRACoL 2013 (CGATS21-2-CRPC6) in CIE L\* a\* b\* space using an IDEAlliance (Chromix/Hutch Color) Curve 4.2.4 application interface with an X-Rite spectrophotometer with an i1iO table. The measured data of each profile were run through this application (Curve 4.2.4). The data were analyzed by using the Verify Tool of the Curve 4.2.4 application to determine the pass/fail of G7 master compliance levels using G7 ColorSpace tolerances (G7 Grayscale, G7 Targeted, and G7 Colorspace). Analyzed data from the experiment revealed that the printed colorimetric values of each profile (G7 Grayscale, G7 Targeted, and G7 Colorspace) are in match (aligned) with the G7 master compliance levels (reference/target) colorimetric values (G7 Grayscale, G7 Targeted, and G7 Colorspace). Therefore, the press run was passed by the Curve 4 application for both the profiles used/tested towards aiming for G7 master compliance.*

## KEY WORDS

G7, Calibration, Color, Device Link, Output Profile, Colorimetry, Gamut, Screening

Haji Naik Dharavath 

Central Connecticut State University, Department of Computer Electronics & Graphics Technology, New Britain, USA

Corresponding author:  
Haji Naik Dharavath  
e-mail: dharavathh@ccsu.edu

First received: 12.2.2020.

Revised: 30.10.2020.

Accepted: 16.11.2020.

## Introduction

G7 stands for grayscale (or gray) plus the seven primary and secondary colors known as the subtractive and additive: Cyan, Magenta, Yellow, Black (CMYK) and Red, Green, Blue (RGB). G7 is a method which specifies cali-

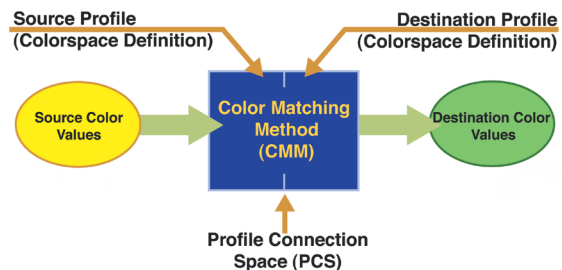
bration procedures for printing visually acceptable colors with an emphasis on matching colorimetrically derived aim-points for the print reproduction processes to print with a common visual appearance. Today, this method (G7) is used in many applications of printing such as offset lithography, flexography, and digital (color laser

or inkjet). It uses a pre-defined one-dimensional neutral print density curve (NPDC) to match neutral tonality/gray balance. G7 specifications are owned by International Digital Enterprise Alliance (International Digital Enterprise Alliance- IDEAlliance, 2014) and the colorimetric formulas of the G7 are defined in the American National Standards Institute and the Committee on Graphic Arts Technology Standards/Technical Report (ANSI/CGATS TR015). Published reports reveal there are three ways G7 master compliance can be achieved: a) output device NPDC to G7 NPDC [P2P251x target image], b) use of output device ICC profile, and c) the use of device link profile (DLP = source as GRACoL2013 ICC profile + the destination device ICC profile). G7 master compliance includes three levels in the G7 master qualification: G7 Grayscale, G7 Targeted, and G7 Colorspace. These levels demonstrate G7 master capabilities of a print facility.

## Review of literature

Digital color print reproduction involves physical/mechanical interaction among the imaging cylinder, dry/liquid toner, and the substrate (Avramovic & Novakovic, 2012). The outcome of this interaction is the color print. Color can be viewed as a science where the optical aspects of color are quantitatively analyzable and measurable. The human eye, however, perceives color more subjectively, which poses a challenge at times for the printing and image reproduction industry. The quality of a color image reproduced through any printing process (digital or traditional) is largely influenced by the properties of paper. While paper is considered a commodity, its properties are a long way from being standardized (Wales, 2009). Additional attributes must be monitored in order to produce quality printed materials; a high-quality color image. The press operator must carefully manage several print parameters, such as the source colors (a source profile of ISO or ANSI standard), press calibration, press characterization (device destination profile), and the screening option. Without controlling these parameters to a print job, a color mismatch would result. A modern and up-to-date commercial printing workflow requires a Color Management System (CMS) to produce a quality color printing. A CMS enables the color producer (printer operator or the designer) to deliver accurate output colors regardless of device color capacities with the use of proper color management techniques (see Figure 1). Analyzing the color image by examining its quantitative attributes eliminates the subjective judgment of color quality evaluation of printed colors or colors in nature. Advancements in science and engineering, however, have allowed print and graphic professionals to apply scientific research methods across printing workflow. Applying these methods heightens the importance of proper print production workflow. Gray balance represents the combination of specific amounts of cyan, magenta, and yellow inks to produce a neutral shade of

gray. With slight increases in cyan pigment required to produce a neutral gray, shifts in hue will occur with any imbalance of these three components. In addition to the color gamut, the gray balance is an additional requirement for pleasing color-reproduction. In large part, the imbalance is due to impurities of the inks, chromaticity deviation of the substrates, or other attributes. To establish the proper gray balance for a specific process, a full set of tint charts can be reproduced. Careful evaluation of the printed tint charts will provide the specific values for that specific reproduction process. The ISO 12647-7 document states that the gray balance can be printed and measured at the CMY overlap (overlap of C = 50%, M = 40%, and Y = 40%). The deviation can be determined from the calculation of  $\Delta H^*$  (deviation of hue,  $h^*$ ) or  $\Delta C^*$  (deviation of chroma,  $c^*$ ) and it requires the colorimetric data of CMY overlap printing from the  $L^* a^* b^*$  model.



» **Figure 1:** Schematic of PCS of CMS (Courtesy of Adobe Systems, Inc.)

## G7 Grayscale

This is the fundamental level of G7 commonly seen in most color print reproduction. Regardless of printing process, if a digital printer or printing press reproduces the defined neutral tone ramp as a neutral gray, then all other colors in the reproduction are believed to be without colorcast. This is determined by printing a target specified on a stable printing system and then measuring the target using the correct ink/toner curves to bring the printing system into alignment with the G7 ideal neutral density curve. Aligning the various reproduction processes and obtaining the same neutral aim points is critical for consistent reproduction.

## G7 Targeted

The secondary level of G7 is achieved when G7 grayscale is matched, and the solid ink measurements for primary, and secondary (CMY and RGB) are also within the G7 target specifications. This can be achieved through the absolute white point or using the substrate-relative conditions. However, G7 Targeted compliance is not limited to the reference print conditions in ISO 12647-2 or in ISO/PAS 15339. The G7-calibrated dataset can be used as a G7 reference print condition. G7 Targeted achievement cer-

tifies that the facility not only conforms to G7 Grayscale, but it can also achieve a higher level of compliance.

## G7 Colorspace

The highest level of G7 compliance, and the most stringent is the G7 Colorspace. It includes all the requirements of the G7 Targeted level and, therefore, the G7 Grayscale level. This also includes the matching of an entire Reference Print Condition (RPC). This level of control demonstrates that the reproduction maintains an extremely tight tolerance throughout the complete color space. An entire TC1617x target is printed and compared against the specific color space with all 1617 patches held to within a tight tolerance. This assures the printing system will reproduce the entire color space, not just the primary and secondary colors of CMYK and RGB. The G7 Colorspace can also relate to either the absolute white point or the substrate-relative aim values.

## Purpose of the research

The purpose of this applied research was to demonstrate the use of a complete color managed workflow (CMW) and meet the specified G7 master compliance levels by creating and using output device ICC profiles. The experiment was conducted in a color managed digital printing workflow (CMDPW) to determine the effect that ODP and DLP have on the G7 master compliance: *Comparison of Compliance with Output Device Profile (ODP) vs. Device Link Profile (DLP) of Multicolor Digital Printing*. It was aimed at achieving the G7 master compliance through an ICC based CMW. As stated earlier, the G7 master compliance print evaluation can be achieved by use of the output device ICC profile (ODP or DLP) for printing. This experiment adopts both methods to achieve the compliance and compare with each other. G7 master compliance includes three compliance levels in the G7 master qualification: G7 Grayscale, G7 Targeted, and G7 Colorspace. These levels demonstrate G7 master capabilities of a print facility. *The G7 calibration method, using the P2P251x target, was NOT considered to derive the device NPDC to compare with G7 NPDC for print (or press) runs 1, 2, 3, etc.*

## Limitations of the Research

For this research, limitations in the technology of the graphics laboratory were acknowledged. Prior to printing and measuring the samples, the digital color output printing device, and color measuring instruments (spectrophotometer and densitometer) were calibrated against the recommended reference. The print conditions associated with this experiment were characterized by, but not restricted to, the inherent limitations: colored images (TC1617x, ISO300, and ISO12647-7) chosen for printing. Additionally, the desired rendering intent

applied, type of digital printer, type of paper, type of toner, resolution, screening technique, color output profiles, and calibration data applied are acknowledged. Several variables affected the facsimile reproduction of color images in the CMDPW, and most were mutually dependent. The scope of the research was limited to the color laser (electrophotographic) digital printing system (printing proof/printing), substrates, types of color measuring devices, color management and control applications (data collection, data analysis, profile creation, and profile inspection) used within the university graphics laboratory. Findings were not expected to be generalizable to other CMDPW environments. It is quite likely, however, that others will find the method used and data collected both useful and meaningful. The research methodology, experimental design, and statistical analysis were selected to align with the purpose of the research, taking into account the aforementioned limitations.

## Research methodology

The digital color printing device used in this experiment is a Konica-Minolta bizHub C6000 Digital Color Press. It uses a Creo IC-307 raster image process (RIP) application (front-end system). A two-page custom test image (12" x 18" size) was created for proofing and printing use for the experiment (See Figures 2 & 2A). The test target contained the following elements: an ISO 300 and generic images for subjective evaluation of color, an ISO 12647-7 Control Strip (2013, three-tier), and a TC1617x target for gamut/profile creation. Glass, G.V. & Hopkins, K. D. (1996) provides an objective method to determine the sample size when the size of the total population is known. The following formula was used to determine the required sample size, which was 80 (n) printed sheets for each group used in this study:

$$n = [ \chi^2 NP (1-P) ] / [ d^2 (N-1) + \chi^2 P (1-P) ] \quad (1)$$

n = the required sample size

$\chi^2$  = the table value of chi-square for 1 degree of freedom at the desired confidence level (3.84)

N = the total population size

P = the population proportion that it is desired to estimate (.50)

d = the degree of accuracy expresses as a proportion (.05)

Table 1 presents the variables, materials, conditions, and equipment associated with this experiment. Colorimetric, Densitometric, and Spectrophotometric data were extracted by using an X-Rite Eye-One Spectrophotometer and an X-Rite i1iO Scanning Spectrophotometer from the color printed samples for the analysis. For both profiles [ODP and DLP (groups, K = 2)], a total of 200 samples of target color images were printed, 100 prints with each profile noted by letter "N" (N = 100).

**Table 1**

Experimental and Controlled Variables

Variable	Material/Condition/Equipment
Test image	Custom Test Target, 2 pages
Control strips/targets	ISO 12647-7 (2013), TC1617x
Other Images	B/W and Color for Subjective Evaluation
Profiling Software	X-Rite i1PROFILER 1.8
Profile Inspection Software	Chromix ColorThink-Pro 3.0
Image Editing Software	Adobe PhotoShop-CC
Page Layout Software	Adobe InDesign-CC
Source Profile (RGB)	Adobe 1998.icc
Destination Profile (CMYK)	Custom, Konica-Minolta.icc
Reference/Source Profile (CMYK)	GRACoL2013.icc
Color Management Module (CMM)	Adobe (ACE) CMM
Rendering Intents	Absolute
Computer & Monitor	Dell OPTIPLEX/LCD
Raster Image Processor (RIP)	Creo IC-307 Print Controller
Printer	Konica-Minolta bizHub C6000 Color Laser
Achieved CMYK SID for all print runs (AM Screen)	C = 1.45; M = 1.36; Y = 0.90; and K = 1.73
Screens and Screen Ruling	AM and 190 LPI
Print Resolution	600 x 600 DPI
Toner	Konica-Minolta Color Laser
Type of Paper Weight/thickness	Hammermill 100LB Matte Coated, Sheetfed
Type of Illumination/Viewing Condition	D50
Color Measurement Device(s)	X-Rite Eye-One PRO Spectrophotometer with Status T, 20 angle, and i1iO Scanning Spectrophotometer
Data Collection/Analysis Software	IDEAlliance/Chromix Curve 4.0 / MS-Excel

Of 100 samples of each group, 80 samples ( $n = 80$ ) were randomly selected and measured, noted by the letter “n” ( $n = 80$ ). This sample size is needed to make sure the reliability of data is accurate. It is well documented that a large sample size is more representative of the sampling population (subjects).

## G7 Compliance for Digital Color Press (printer)

Prior to printing the patches/target image, the printer was calibrated for amplitude modulated (AM) screening according to its manufacturer specifications. A calibration process means standardizing the performance of the devices according to the device manufacturer specifications so that the results of the devices are repeatable. The calibration curve consists of the maximum printable densities of each color (CMYK) on the press (See Figure 3). Test target TC1617x was used for the output device profile creation process.

In a generic color managed digital printing workflow, digital front-end (DFE) platforms (raster image processor or RIP) of digital printers (or presses) offer opportunities for the user (or press operator) to manipulate the output color quality to meet the expected demand of the customer. The AM screening option offered the ability to set printer resolution at 600 DPI, 1200 DPI, and 2400 DPI. But as a choice only the 600 DPI resolution was

selected for both profiles to keep the print parameters/variables consistent throughout the experiment.

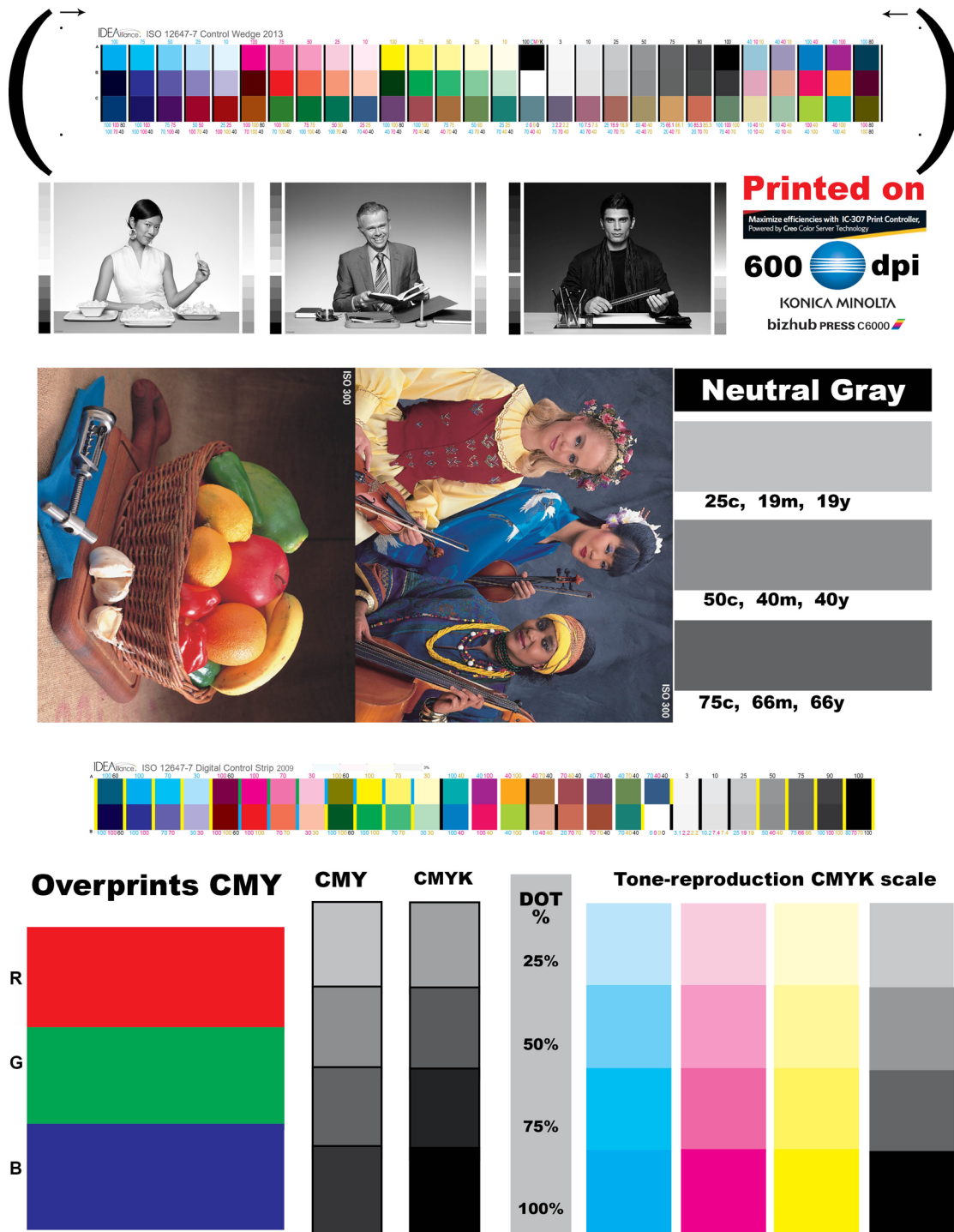
## Output Device Profile (ODP) for G7 Compliance

The target image (TC1617x) was placed into an Adobe InDesign-CC layout of 12” W x 18” H size and a .PDF file was created without any image/color compression technique (see Figures 2 & 2A). Hammermill brand, 100 LB matte-coated digital color printing paper 12” x 18” was used for printing the target image in the experiment. Prior to printing the TC1617x target (See Figure 2A) for creating the device profile, the printer was calibrated. The calibration data (range of CMYK densities) were saved in the calibration lookup tables of the raster image processor (RIP) and a calibration curve was created (See Figure 3). A total of 100 sheets/copies of TC1617x were printed with the calibration curve attached. Also, an amplitude modulated (AM) halftone screening technique with 190 lines per inch (LPI) and 600 DPI as the printer resolution was applied during the printing of the target. No color management or color correction techniques were applied during the printing. Printed patches of TC1617x were measured in CIE  $L^* a^* b^*$  space using the i1PROFILER application with an X-Rite spectrophotometer with an i1iO table and the data were run through this application. The printer profile (Output Device Profile) was created and stored at the right location on the computer.

The profile format version is 4.00 and it is considered as the Output Device Profile (ODP) of AM screening. This profile was used as a destination profile

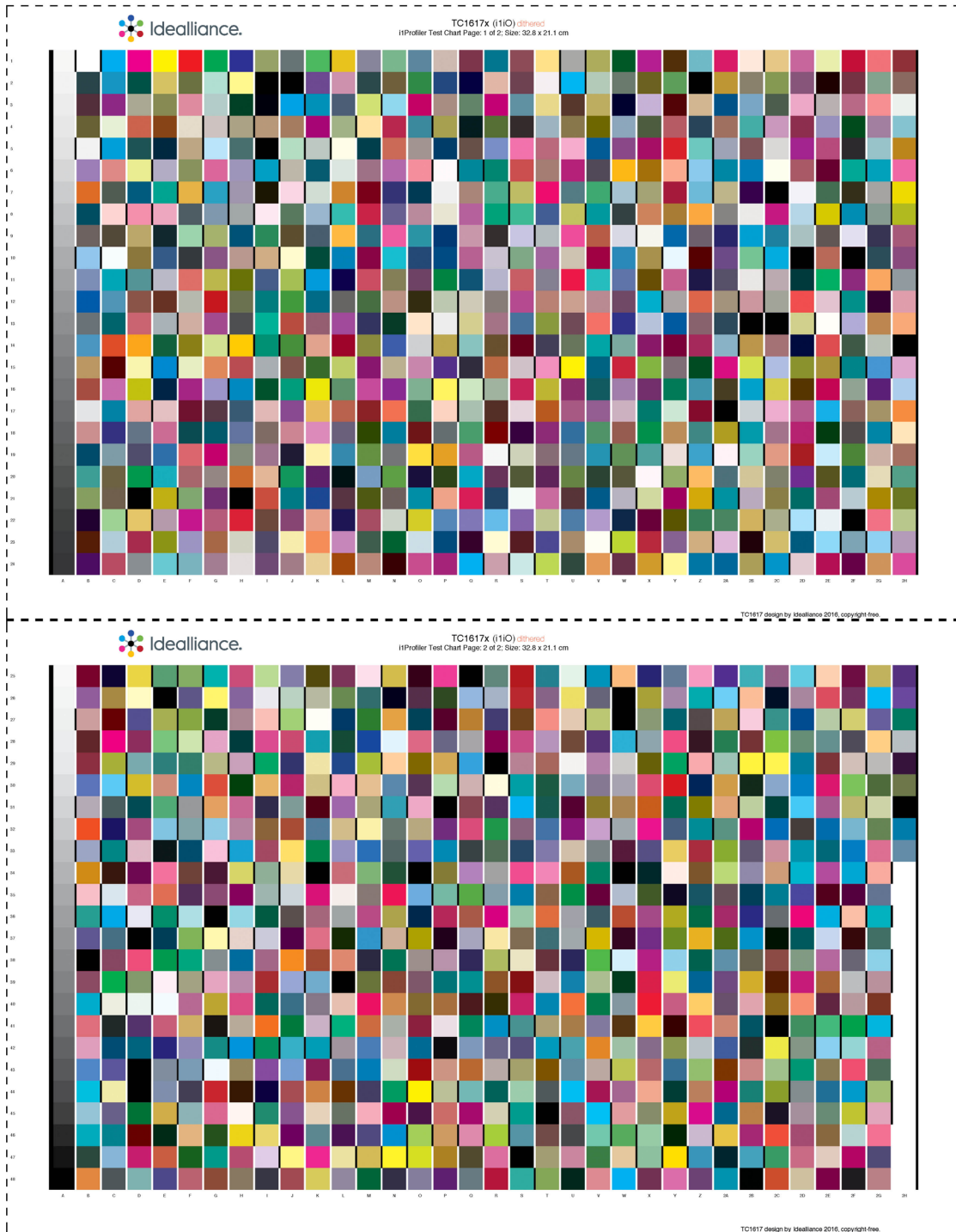
(DP) in the workflow. The source profile (SP) used in the experiment is a GRACoL2013 for characterized reference printing conditions-6 (CRPC-6).

## Aiming for G7 Master Compliance through a Color Managed Workflow: Comparison of Compliance with Output Device Profile (ODP) vs. Device Link Profile (DLP) of Multicolor Digital Printing



» Figure 2: Test Image for the experiment (PAGE 01)

# Aiming for G7 Master Compliance through a Color Managed Workflow: Comparison of Compliance with Output Device Profile (ODP) vs. Device Link Profile (DLP) of Multicolor Digital Printing



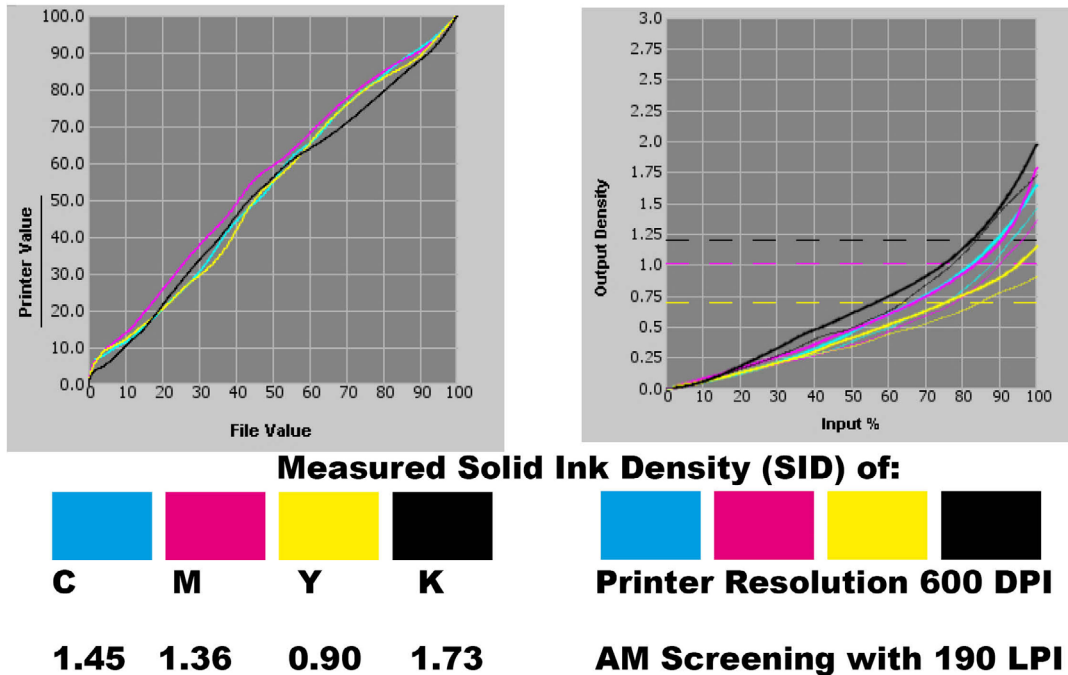
» **Figure 2A:** Test Image for the experiment (PAGE 02)

## Device Link Profile (DLP) for G7 Compliance

In a generic color managed digital printing workflow, the color space of the input device (RGB) is transformed

to the color space of the output device (CMYK) via the device independent  $L^*a^*b^*$  color space or the profile connection space (PCS). This process (the DLP) requires two different profiles, namely a source (RGB) profile and a destination (CMYK) profile. There is no PCS in a color

## PRINTER CALIBRATION FOR G7 MASTER COMPLIANCE



» **Figure 3:** Calibration of a Digital Press

managed digital printing workflow which uses a DLP. The source and the ODP are directly linked. Device link profiles are most commonly applied to direct CMYK-to-CMYK color transformations. An X-Rite i1PROFILER application was used to create the DLP by merging the source profile (GRACoL2013) and the ODP of the digital press. In this scenario the source profile used was GRACoL2013 for characterized reference printing conditions-6 (CRPC-6) and the destination device profile used was the ODP (Konica-Minolta C6000 bizHUB digital color press). So, the DLP used contained the two profiles.

### Printing for G7 Compliance

Each profile (ODP vs DLP) used in the experiment was considered as a group, noted by letter “K” (K = 2). A group involves a set of print parameters, such as: a digital halftone screening technique [amplitude modulate (AM)], the calibration curve (of AM screened), a color source profile [General Requirements for Applications in Commercial offset Lithography for characterized reference printing conditions-6 (GRACoL2013 for CRPC-6)] or a DLP, and a color destination profile of a digital press (AM screened) or a DLP. As parameters illustrated in the figure 4 (*Schematic Illustration of Sequence of Print Parameters for G7 Compliance*), test target of 12” x 18” was printed for use in the experiment.

#### Press Run 1: Printing with ODP

A total of 100 sheets/samples were printed. The digital press calibration curve, AM screening destination profile, and the source profile (GRACoL 2013) all were

applied during the printing. A total of 80 randomly pulled printed copies of TC1617x printed target images were measured against G7 ColorSpace GRACoL 2013 (CGATS21-2-CRPC6) in CIE L\* a\* b\* space using an IDE-Alliance (Chromix/Hutch Color) Curve 4.2.4 application interface with an X-Rite spectrophotometer with an i1i0 table. The measured data were combined/averaged to run through this application (Curve 4.2.4). The combined data set was analyzed by using the Verify Tool of the application to determine the pass/fail of G7 master compliance levels using G7 ColorSpace tolerances. Analyzed data from the experiment revealed that the printed colorimetric values (G7 Grayscale, G7 Targeted, and G7 Colorspace) are in match with the G7 master compliance levels (reference/target) colorimetric values (G7 Grayscale, G7 Targeted, and G7 Colorspace).

#### Press Run 2: Printing with DLP

A custom test target from the press run one was used for proofing and printing use for the experiment. A total of 100 sheets/samples were printed by enabling the color management technique for the use of DLP at the RIP. The digital press calibration curve and the DLP both were applied during the printing. A total of 80 randomly pulled printed copies of TC1617x printed target images were measured against G7 ColorSpace GRACoL 2013 (CGATS21-2-CRPC6) in CIE L\* a\* b\* space using an IDEAlliance (Chromix/Hutch Color) Curve 4.2.4 application interface with an X-Rite spectrophotometer with an i1i0 table and the data were combined to run through this application. Color measurement and analysis steps used in the printing with ODP process

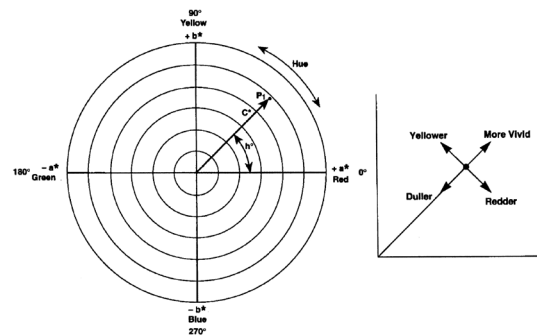
(previous section) were applied/followed for printing with DLP process. Printed colors with DLP were also found to be very accurate and the process was efficient.

## Data analysis & research findings

The colorimetric computation methods for G7 compliance were used to analyze the collected data and presented in the following pages/tables. Subjective judgment on color difference or any deviation was not used in this particular study because the subjective judgment of color difference could differ from person to person. For example, people see colors in an image not by isolating one or two colors at a time (Goodhard & Wilhelm, 2003), but by mentally processing contextual relationships between colors where the changes in lightness (value), hue, and chroma (saturation) contribute independently to the visual detection of spatial patterns in the image (Goodhard & Wilhelm, 2003). Instruments, such as colorimeters and spectrophotometers, eliminate subjective errors of color evaluation perceived by human beings. In comparing the color differences between two colors, a higher deviation ( $\Delta E$  or  $\Delta H$  or the  $\Delta C$ ) is an indication that there is more color difference and a lesser deviation ( $\Delta E$  or  $\Delta H$  or the  $\Delta C$ ) is an indication of less color difference. In this scenario of the color measuring/evaluation stage, a consistent and standardized light source (D50 or D65) and angle of viewing ( $2^\circ$  or  $10^\circ$ ) are important.

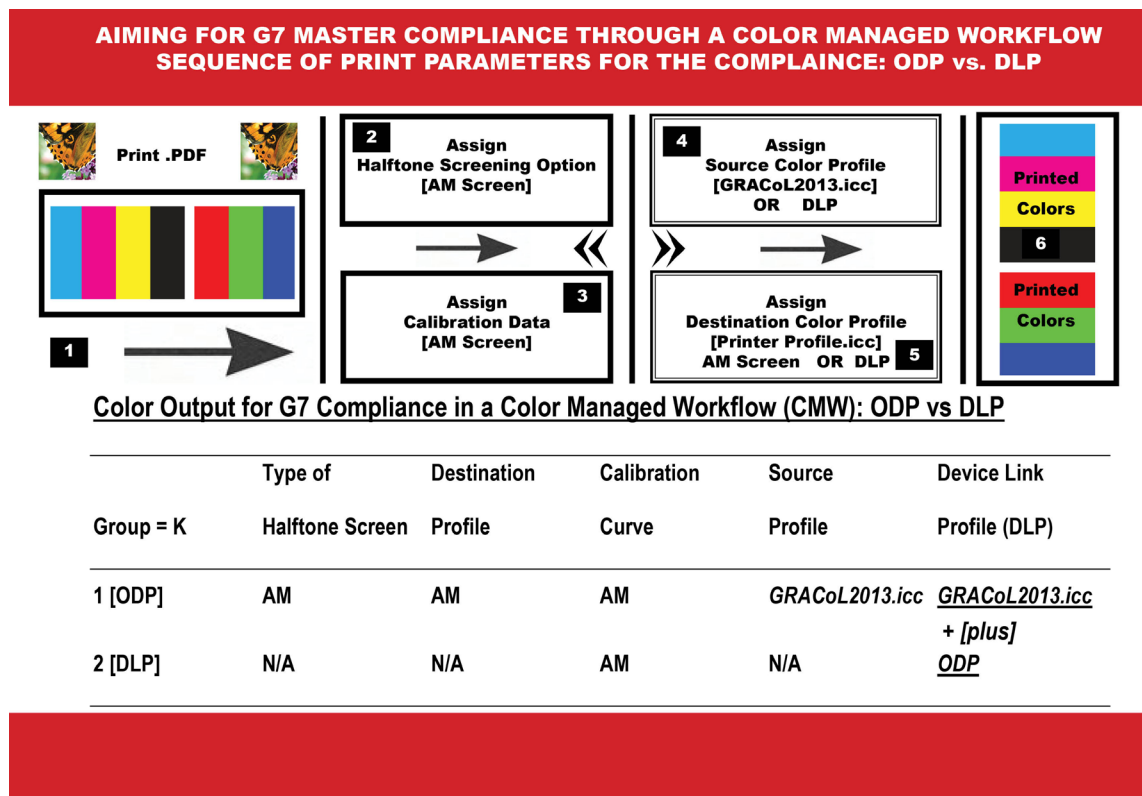
## CIE L\* a\* b\*, Delta L\* Delta E and Delta Chroma ( $\Delta L$ , $\Delta E$ and $\Delta C$ )

Colorimetric values of printed colors against original colors and the deviations (Delta's) can be used to determine the visual variation in overall colors, hue, chroma, and lightness. The  $a^*$ ,  $b^*$  coordinates correspond approximately to the dimensions of redness – greenness and yellowness – blueness respectively in the CIE L\*  $a^*$   $b^*$  color space and are orthogonal to the L\* dimension. Hence, a color value whose coordinates  $a^* = b^* = 0$  is considered achromatic regardless of its L\* value. Calculation of  $\Delta H^*$  requires colorimetric data from the L\*  $a^*$   $b^*$  model.



» **Figure 5:** Schematic of L\*  $a^*$   $b^*$  &  $c^*$ ,  $h^*$  Coordinates

Metric hue angle  $h^*$  and  $C^*$  are defined by the following formulas (Morovic, Green & MacDonald, 2002).



» **Figure 4:** Schematic Illustration of Sequence of Print Parameters for G7 Compliance



$$\text{Metric hue angle: } h_{*ab} = \tan^{-1} \left( \frac{b^*}{a^*} \right) \quad (2)$$

Where:  $a^*$ ,  $b^*$  are chromaticity coordinates in  $L^* a^* b^*$  color space

$$\text{Chroma (C*)} = [a^2 + b^2]^{1/2} \quad (3)$$

Where:  $a^*$ ,  $b^*$  are chromaticity coordinates in  $L^* a^* b^*$  color space

Calculation of  $\Delta C^*$  (of two colors) and  $\Delta L^*$  requires colorimetric data from the  $L^* a^* b^*$  model. Difference in the chroma  $C^*$  of two colors (Reference vs. Printed) can be calculated by using the following formula (Green et al., 2002).

$$\Delta \text{Chroma } (\Delta C) = C^*_{1} - C^*_{2} \quad (4)$$

Where: 1 =  $C^*$  of Reference Color and 2 =  $C^*$  of Printed Color

Assessment of color is more than a numeric expression. It is an assessment of the difference in the color sensation (delta) from a known standard. In the CIELAB color model, two colors can be compared and differentiated. The expression for these color differences is expressed as  $\Delta E$  (Delta E or Difference in Color Sensation). The following equation is used to calculate the  $\Delta E$  (Committee for Graphic Arts Technologies Standards – CGATS, 2003)

$$\Delta E^* = \sqrt{(L_1 - L_2)^2 + (a_1 - a_2)^2 + (b_1 - b_2)^2} \quad (5)$$

Where: 1 = Reference Color and 2 = Printed Color

Chromaticness difference ( $\Delta \text{Ch}$ ) is the difference between the reference chroma ( $a^*1$  and  $b^*1$ ) and the measured chroma ( $a^*2$  and  $b^*2$ ) of a gray balance control patch (C50, M40, Y40). Weighted Delta Chroma ( $w\Delta \text{Ch}$ ) is the delta Ch value after it is passed through a weighting curve that reduces the significance of Ch errors in the darker regions of the color. The weighting function is defined in the G7 specifications ([Technical Report (TR) 015] and the G7 master pass/fail document as follows (Chromix, Inc., 2019):

$$w\Delta \text{Ch} = \Delta \text{Ch} \times [1 - \max(0, (\% - 50) / 50 \times 0.75)] \quad (6)$$

Delta  $L^*$  ( $\Delta L^*$ ) is the difference in the lightness between the reference and measured sample lightness regardless of any color. This makes  $\Delta L^*$  the perfect metric for measuring tonality [Neutral Print Density Curve (NPDC)] error in G7. Colorimetrically,  $\Delta L^*$  is the result of subtracting the  $L^*$  of measured sample value from the reference  $L^*$ , as follows:

$$\Delta L^* = L^*_{1} - L^*_{2} \quad (7)$$

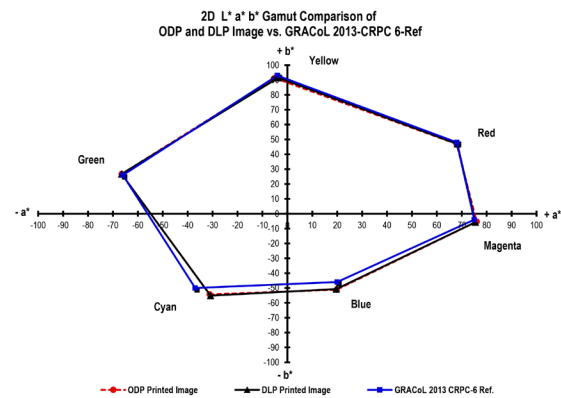
Where: 1 =  $L^*$  of Reference Color and 2 =  $L^*$  of Printed Color

Weighted Delta  $L^*$  ( $w\Delta L^*$ ) is the delta  $L^*$  value after it is passed through a weighting curve that reduces the significance of  $L^*$  errors in the darker regions of the color. The weighting function is identical to that for  $w\Delta \text{Ch}$ , as follows (Chromix, Inc., 2019):

$$w\Delta L^* = \Delta L^* \times [1 - \max(0, (\% - 50) / 50 \times 0.75)] \quad (8)$$

## Overall Color Variation ( $\Delta E$ ) of ODP (TC1617x image) vs. GRACoL 2013 Ref.

The CIE  $L^* a^* b^*$  values associated with the CMYK+RGB colors of printed image with ODP vs. G7 ColorSpace-GRACoL 2013 [CGATS21-2-CRPC6 (reference)] are compiled in Table 2. Numerical color differences ( $\Delta E$ ) were found when comparing the colors of printed image vs. G7 ColorSpace at all seven colors (CMYK+RGB). Also, noticeable visual color differences were found in the solid color area [lightness, color hue and chroma]. Overall, both groups of images have similar colors (see Figures 6, 7, 8 and 9) with the exception of the printed image consisting of higher  $L^*$  for red, magenta, and green, etc. This results in producing the higher  $\Delta E$  for these colors.



» **Figure 6:** Image (colors) printed with ODP and DLP vs. GRACoL 2013-CRPC-6 Ref.

This higher color deviation (red, magenta and green) could be the result of the substrate (paper) and toner used (age, condition, quality, etc.). These are the darker colors which produced lower  $L^*$  value and in turn affected the higher deviation.

The 2D color gamut comparison (see Figures 6, 7, 8 and 9) reveals that the colors of the printed image closely match the reference colors. The goal was to determine the deviations among various attributes of color between these two groups of colors.

The comparison is an indication that, in a color managed workflow (CMW), color matching of a target image can be achieved from device to device regardless of device color characterization and original colors. Subjective judgment was not used for the color comparison.

**Table 2**

Overall Color Variation of CMYK+RGB: Printed Image (TC1617x) vs. G7 ColorSpace

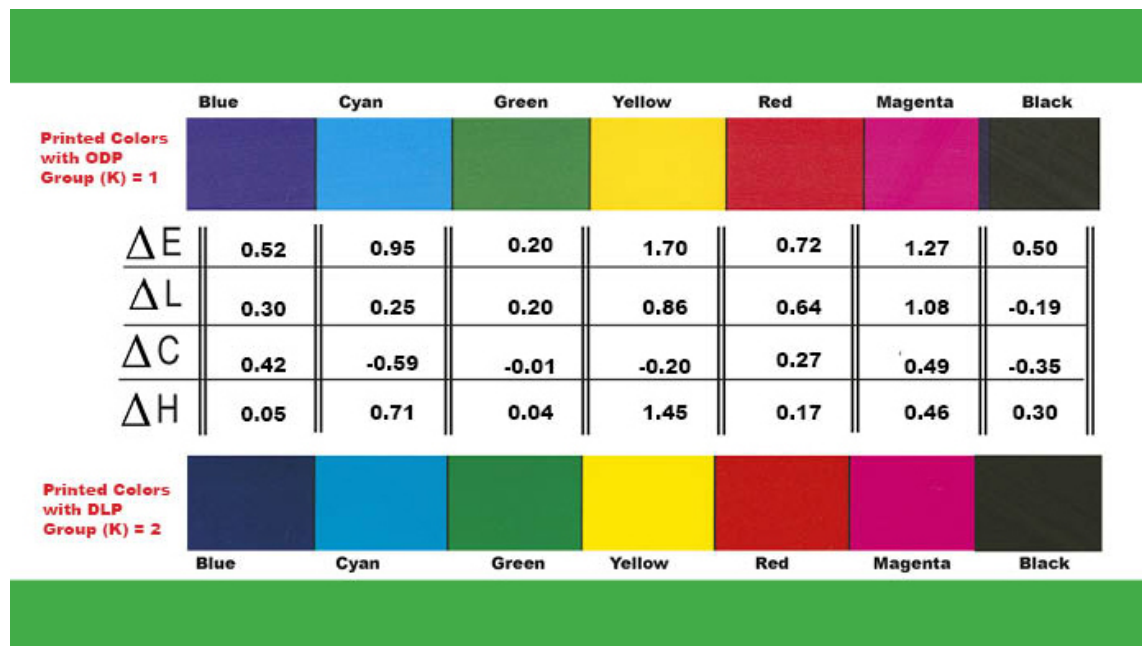
Color(s)	ODP Printed Image			G7 ColorSpace / Target			Color Difference $\Delta E$
	L*	a*	b*	L*	a*	b*	
	Color 1 N = 80			Color 2 N = N/A			
White (W)	97.22	2.79	-9.45	97.22	2.79	-9.45	0.00
Cyan	57.22	-31.17	-54.27	57.40	-36.88	-55.84	2.06
Magenta	51.19	75.97	-5.30	49.22	77.93	-7.09	2.13
Yellow	90.86	-5.06	91.29	91.10	-2.43	92.93	1.47
Black (K)	13.07	0.47	0.07	16.30	0.24	-0.74	2.29
Red	50.50	67.90	46.95	48.19	70.74	48.26	2.40
Green	53.56	-66.51	26.72	51.26	-66.87	24.49	2.45
Blue	27.06	19.75	-51.14	25.62	21.19	-50.24	1.71
TAC 300	24.27	0.01	-1.95	23.56	0.45	-1.34	1.01
TAC 400	9.91	0.72	-1.04	8.99	0.17	0.61	1.90

**Overall Color Variation ( $\Delta E$ ) of DLP (TC1617x image) vs. GRACoL 2013 Ref.**

The CIE L\* a\* b\* values associated with the CMYK+RGB colors printed image with DLP vs. G7 ColorSpace-GRACoL 2013 [CGATS21-2-CRPC6 (reference)] are compiled in Table 3. Numerical color differences ( $\Delta E$ ) were found when comparing the colors of the DLP printed image vs. G7 ColorSpace at all seven colors (CMYK+RGB). Also, noticeable visual color differences were found in the solid color area [lightness, color hue and chroma]. Overall, both groups of images have similar colors (see Figures 6, 7, 8 and 9) with the exception of the printed image consisting of higher L\* for green. This results in producing the higher  $\Delta E$  for these colors. This higher color

deviation (green and cyan) could be the result of the applied DLP. Green is the darker color which produced lower L\* value and in turn affected the higher deviation.

The 2D color gamut comparison (see Figures 6, 7, 8 and 9) reveals that the colors of the printed image closely match the reference colors. The goal was to determine the deviations among various attributes of color between these two groups of colors. The comparison is an indication that, in a color managed workflow (CMW), G7 master compliance for color matching of a target image can be achieved. Subjective judgment was not used for the color comparison. In addition to the colorimetric comparison of individual colors (Tables 3 and 4) of both groups with G7 ColorSpace, the G7 master compliance



» **Figure 7:** Color Variations ( $\Delta L$ ,  $\Delta C^*$ ,  $\Delta H$ , and  $\Delta E$ ) of ODP vs. DLP [Colors presented in this chart do not represent actual  $K_1$  vs.  $K_2$  colors]

colorimetric deviation ( $w\Delta Ch$  and  $w\Delta L$ ) values for all the three levels (G7 Grayscale, G7 Targeted and G7 ColorSpace) are in close match with the established tolerances for the G7 (see Table 4, 4A, and 4B). This includes the Neutral Print Density Curve [NPDC (CMY)] and NPDC (K).

### Four Deviations ( $\Delta L$ , $\Delta E$ , $\Delta C^*$ & $\Delta H^*$ ) of OPD vs DLP

Chroma and Hue Variation ( $\Delta C^*$  &  $\Delta H^*$ ) values of the colors printed with OPD vs. color printed with DLP are presented in figure 8. Interpreting  $L^* a^* b^*$  color space data is similar to  $L^* a^* b^*$ , but the data describes col-

or differently using cylindrical coordinates instead of rectangular coordinates (see Figures 6, 7, 8 and 9). In this color space,  $L^*$  indicates lightness,  $C^*$  represents chroma, and  $h^*$  is the hue angle of the color. Deltas (deviations) for lightness ( $\Delta L^*$ ), chroma ( $\Delta C^*$ ), and hue ( $\Delta H^*$ ) may be positive (+) or negative (-). When compared, the printed colors of OPD vs. DLP are very similar to each other (see Figures 6, 7, 8 and 9).

The +  $\Delta L^*$  values indicate that the remaining colors are lighter. The -  $\Delta C^*$  of cyan, green, and yellow colors indicate that they are duller in comparison with the other of the same colors in the reproduction.

**Table 3**

Overall Color Variation of CMYK+RGB: Printed Image (TC1617x) vs. G7 ColorSpace

Color(s)	DLP Printed Image			G7 ColorSpace / Target			Color Difference $\Delta E$
	L*	a*	b*	L*	a*	b*	
	Color 1 N = 80			Color 2 N = N/A			
White (W)	97.06	2.79	-9.33	97.06	2.79	-9.33	0.00
Cyan	56.75	-30.84	-55.13	57.29	-36.82	-55.65	2.28
Magenta	50.11	75.45	-5.72	49.12	77.81	-7.02	1.20
Yellow	90.00	-3.62	91.56	90.95	-2.43	92.82	0.91
Black (K)	13.26	0.78	-0.27	16.28	0.24	-0.72	2.18
Red	49.86	68.22	46.96	48.10	70.63	46.21	1.84
Green	53.36	-66.51	26.76	51.17	-66.76	24.49	2.36
Blue	26.76	19.64	-50.73	25.58	21.14	-50.08	1.54
TAC 300	24.31	0.42	-2.52	23.52	0.45	-1.31	1.26
TAC 400	9.84	0.93	-0.36	8.99	0.17	0.60	1.56

**Table 4**

Master Compliance Levels G7 Grayscale of OPD, DLP vs. G7

All Metrics	Black (K)	CMY (Overlap)		G7 Tolerance
	$w\Delta L^*$	$w\Delta L^*$	$w\Delta Ch$	
<b>G7 Grayscale of ODP/Printed Image (Tonality/Gray Balance)</b>				
Average	0.97	0.31	0.81	1.50
Maximum	2.34	0.92	1.90	3.00
<b>G7 Grayscale of DLP/Printed Image (Tonality/Gray Balance)</b>				
Average	0.88	0.32	1.06	1.50
Maximum	2.79	0.92	2.7	3.00

**Table 4A:**

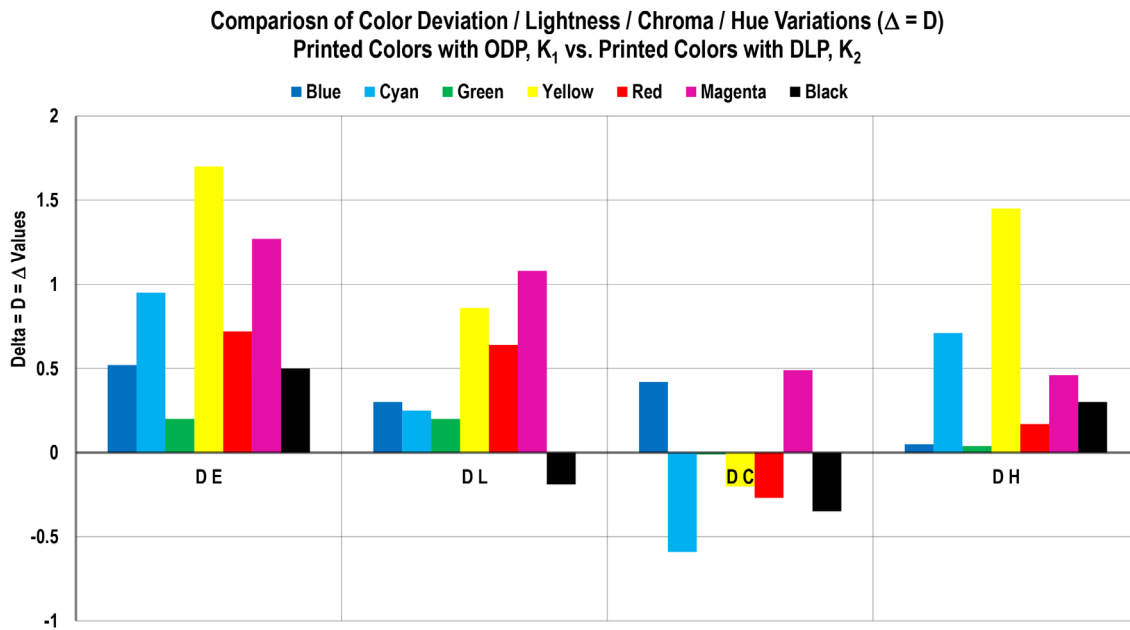
G7 Master Compliance Levels G7 Targeted of ODP, DLP vs. G7

All Metrics	$\Delta E$ 2000	G7 Tolerance	Maximum	G7 Tolerance
<b>G7 Targeted of ODP/Printed Image</b>				
Substrate	0.00	3.00		
K	2.29	5.00		
CMY			2.13	3.5
RGB			2.45	4.3
<b>G7 Targeted of DLP/Printed Image</b>				
Substrate	0.00	3.00		
K	2.18	5.00		
CMY			2.28	3.5
RGB			2.36	4.3

**Table 4B:**

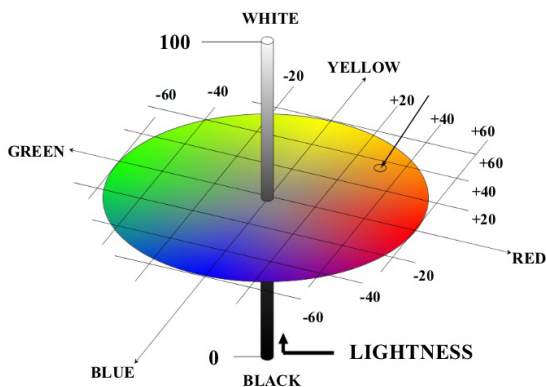
G7 Master Compliance Levels G7 Colorspace of ODP, DLP vs. G7

All Metrics	$\Delta E$ 2000	G7 Tolerance
<b>G7 Colorspace of ODP/Printed Image</b>		
Average	1.18	3.5
95%	2.21	5.0
<b>G7 Colorspace of DLP/Printed Image</b>		
Average	1.12	3.5
95%	2.15	5.0



» **Figure 8:** Visual Color Variations ( $\Delta L$ ,  $\Delta C^*$ ,  $\Delta H$ , and  $\Delta E$ ) of ODP vs. DLP [Colors presented in this chart do not represent actual  $K_1$  vs.  $K_2$  colors]

The +  $\Delta C^*$  of blue, red and magenta colors are brighter. The positive  $\Delta H^*$  values of all the colors of ODP vs DLP indicate that these colors fall in counterclockwise (or clockwise) to one another, meaning these colors are almost identical visually.



» **Figure 9:** CIE 2D / (3D)  $L^* c^* h^*$  Color Coordinates (Courtesy of Google Images)

## Summary/conclusions

This experiment used an output device ICC profile to achieve the compliance. G7 master compliance includes three compliance levels in the G7 master qualification: G7 Grayscale, G7 Targeted, and G7 Colorspace. These levels demonstrate G7 master capabilities of a print facility. The experiment was conducted in a Color Managed Digital Printing Workflow (CMDPW). It was aimed at achieving the G7 master compliance through an ICC based color managed workflow (CMW) by applying the ODP and DLP as two independent groups.

The G7 calibration method, using the P2P251x target, was NOT used to derive the device NPDC to compare with G7 NPDC for print (or press) runs 1, 2, 3, etc.

The conclusions of this study are based upon an analysis of colorimetric data, visual assessment, and associated findings. The experiment analyzed the comparison of G7 compliance of two print profiles (ODP and DLP). The guiding objectives of this study allowed testing of an accepted color management practice to gain a better understanding of the presumptions associated with the application of an output device profile (ODP) and device link profile (DLP). The experiment examined the importance of calibration, characterization and the color evaluation processes of the digital press which was capable of printing colors to match or be in proximity of G7 master compliance levels.

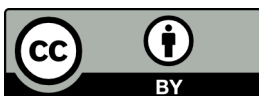
It is evident that integration of device profiles (ODP or DLP) is important in a CMW and it also enables/allows the workflow process to meet the G7 compliance levels via an ICC based CMW, instead of using G7 calibration methodology. Selection of output profile (ODP or DLP) is based on individual preference because printing with both the profiles proved to be within the G7 compliance (G7 Grayscale, G7 Targeted, and G7 Colorspace). Use of DLP reduces the number of steps to follow in the workflow at the RIP of the digital press for managing the color printing because most of the print parameters (calibration, destination profile, source profile, screening option, etc.) are already embedded in the DLP. This study represented specific printing or testing conditions. The images, printer, instrument, software, and paper that were utilized are important factors to consider when evaluating the results. The findings of the study cannot be

---

generalized to other digital printing workflow. However, other graphic arts educators, industry professionals, and researchers may find this study meaningful and useful.

## References

- Avramovic, D. & Novakovic, D. (2012) Influence of Printing Surface Attributes on Print Quality in Electrophotography. *Technical Gazette*. 19 (2), 295-301.
- Chromix, Inc. (2019) *Curve 4.2.4 Software Manual*. Seattle, Chromix, Inc.
- Committee for Graphic Arts Technologies Standards-CGATS (2003) *Graphic technology – spectral measurement and colorimetric computation for graphic arts image*. (ANSI/CGATS.5-2003). Reston, The Association for Suppliers of Printing and Publishing Technologies.
- Glass, G. V. & Hopkins, K. D. (1996) *Statistical Methods in Education & Psychology*. Boston, Allyn & Bacon.
- Goodhard, M. M. & Wilhelm, H. (2003) *A new test method based on CIELAB colorimetry for evaluating the permanence of pictorial images*. Wilhelm Imaging Research, Inc. Available from: <http://www.wilhelm-research.com> [Accessed: 20th August 2019].
- International Digital Enterprise Alliance- IDEAlliance (2014) *IDEAlliance Guide to Print Production*. Alexandria, IDEAlliance.
- Morovic, J., Green, P. & MacDonald, L. (2002) *Color Engineering*. New York, John Wiley & Sons. pp. 297-314.
- Wales, T. (2009) *Paper: The Fifth Color*. Alexandria, IPA Bulletin- International Prepress Association (IPA)- Now part of IDEAlliance. Available from: [http://idealliance.org/files/2008\\_03tech.pdf](http://idealliance.org/files/2008_03tech.pdf) [Accessed: 20th August 2019].



© 2021 Authors. Published by the University of Novi Sad, Faculty of Technical Sciences, Department of Graphic Engineering and Design. This article is an open access article distributed under the terms and conditions of the Creative Commons Attribution license 3.0 Serbia (<http://creativecommons.org/licenses/by/3.0/rs/>).





# Optimization of flexographic print properties on ecologically favorable paper substrates

## ABSTRACT

*Nowadays, the attention in many industries is shifting towards the problem of waste overproduction and production of the waste in general. This study aimed to find an alternative approach to the production of packaging which will be environmentally friendly and at the same time optimal in terms of the print quality. This was accomplished by using the minimal needed amount of material for the production of packaging and adjusting the parameters of the flexographic printing process to achieve the desired visual impression of the print. The designed motive for the packaging was printed on five different recycled papers, following the guidelines of sustainable design. Printing was performed on each recycled paper with different printing pressures (50N, 150N, and 400N). Smoothness was measured on each paper; and for every printed sample, colorimetric measurements and thickness of the lines in positive and negative were measured. Print contrast for each print was calculated, and microscopy of fine printed elements was performed. All chosen papers except one had average smoothness of up to 3.2 s (the smoothest paper had the average smoothness value of 54.72 s). Smoothness results influenced the printed line widths. Specifically, when increasing the printing pressure, a significant deformation of the line width has occurred on all papers except the smoothest one (deformations of the lines printed in positive were up to 400  $\mu\text{m}$  for rough papers compared to maximum of 60  $\mu\text{m}$  for lines printed on the smoother paper). Similar results were obtained for the lines printed in negative. Furthermore, legibility of the printed typographic elements of 4pt size was significantly influenced by the smoothness of the paper. Elements printed on the smoothest paper have displayed the negligible deformations when changing the printing pressure. For other papers, elements in positive were optimally printed by 50 N pressure, and elements in negative by the pressure of 400 N. The results of this research have enabled the optimization of the flexographic printing process when using each of the five types of recycled papers. Furthermore, the presented qualitative and colorimetric parameters of the prints enabled the assessment of the applicability of used papers as printing substrates for ecologically favorable packaging.*

## KEY WORDS

Recycled paper, flexography, printing pressure, colorimetry, line width

Tamara Tomašegović   
Jesenska Pibernik   
Sanja Mahović Poljaček   
Anđela Madžar

University of Zagreb,  
Faculty of Graphic Arts,  
Zagreb, Croatia

Corresponding author:  
Tamara Tomašegović  
e-mail: [ttomaseg@grf.hr](mailto:ttomaseg@grf.hr)

First received: 14.10.2020.

Revised: 9.1.2021.

Accepted: 14.1.2021.

## Introduction

The packaging is nowadays a fast-growing and fast-developing area in graphic technology. Special attention when designing the packaging product and choosing the materials for the packaging is being given to the

ecological aspect of the final product. The principle of sustainable packaging is emphasizing the need for the usage of ecologically favorable materials (Dahlbo et al., 2018; Kaiser, Schmid & Schlummer, 2017). This includes biodegradable and recycled materials (Moustafa et al., 2019; Marrez, Abdelhamid & Darwesh, 2019). Further-

more, the printing process should require a minimal amount of toxic chemicals. For example, printing plates used in the reproduction should be produced without using harmful compounds such as developing agents, and the usage of ecologically harmful printing inks should be avoided whenever possible (Tomašegović et al., 2020; Izdebska, Żółek-Tryznowska, & Świętoński, 2015). Printing substrates for packaging that are eco-friendly are made of recycled and/or biodegradable materials such as recycled (and uncoated) papers, cellophane, PLA, PCL, and other polymeric materials (Ivanković et al., 2017; Mohamed & Yusoh, 2015; Mraović et al., 2014; Pivnenko, Eriksson and Astrup, 2014). The potential issues which occur when printing on eco-friendly substrates, especially recycled papers are printability and the quality of the print (El-Sherif et al., 2019; Aydemir, 2016). Since recycled papers are usually not coated, the absorptivity and roughness of the substrate can cause problems with the ink spreading, absorption, and consequently the inability to print fine elements such as thin lines and small font sizes (Bates et al., 2020; Miljković, Valdec & Matijević, 2018). Furthermore, many recycled papers have their specific shade which influences the colorimetric properties of the printed ink. Therefore, color deviations from the original ink color can be noticeable and even decrease the contrast between the substrate and printing ink, causing illegibility.

This research aimed to optimize the flexographic printing process used for printing on different recycled papers. Flexography was chosen as a printing technique because the elastomeric printing plate can adjust to rough printing substrates (Tomašegović et al., 2016). The process of the printing plate production can be aligned with ecological guidelines by using the laser-engraved EPDM printing plate and eliminating the need for harmful solvents. Modification of the printing pressure and analysis of the qualitative properties of the print on each recycled paper resulted in the recommendations for the application of used paper for specific types of motives on the packaging.

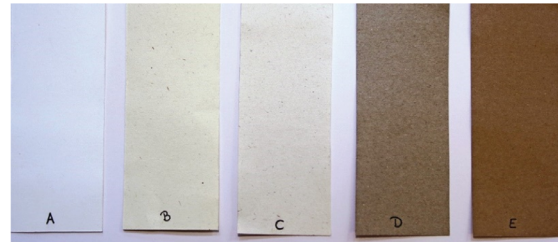
## Experimental

### Materials and methodology

To respect the sustainable design and ecological favourability of the packaging production, five different recycled paper was used as a printing substrate for packaging (Figure 1). The properties of each paper are listed in Table 1.

Papers were cut to samples of 5 x 70 cm and conditioned 24 hours before printing. The printing process was carried out using IGT Printability Tester F1 (IGT Testing Systems, 2016) in the laboratory, at a relative humidity of 55% and 23 °C. Anilox roller of 140 l/cm and 7.5 ml/m<sup>2</sup>

was used. Anilox pressure was set to 300 N, and printing speed was set to 0.3 m/s. UV-curable ink, Pantone 363 U was used. Printing pressure was varied in the printing process – it was set to 50 N, 150 N, and 400 N. In that way, 3 sets of printed samples were obtained for each paper. In the reproduction process, the ethylene propylene diene monomer (EPDM) printing plate was used. The production of the EPDM printing plate does not include any solvents, since the image is transferred to the printing plate utilizing laser engraving, without any developing processes (Wienke et al., 2020).



» **Figure 1:** Recycled papers used as a printing substrate

**Table 1**

Grammage of the recycled papers used in the research

	A	B	C	D	E
<b>Brand</b>	MOHAWK	FLORA	FLORA	SCHOELLERS	SCHOELLERS
<b>Grammage (g/m<sup>2</sup>)</b>	220	130	100	140	140

The smoothness of the paper was measured ten times on each sample according to Bekk method on a PTI-Line Bekk device. The smoothness test was carried out according to TAPPI standard T 479. Samples were placed on the glass plate, above which the measuring head is located. The measuring head pressed the sample with a weight of 10 kg. The vacuum pump adjusted the air tank to a target pressure of 50.7 kPa. Depending on the smoothness of the test sample, the air remaining between the paper surface and the glass plate was transferred to the tank, until the pressure dropped to 48.0 kPa. The time it takes for the air volume of 10 mL to achieve a pressure of 48.0 kPa provided the smoothness value expressed in seconds. A longer time indicates a smoother surface (Cigula, Tomašegović & Hudika, 2019).

Colorimetric measurements were performed employing an X-rite eXact spectrophotometer (X-Rite, 2018). Measurements were performed 10 times on different parts of each printed sample, with the measurement conditions set to illuminant D50, a standard observer of 2° and filter M1. CIE L\*, a\*, and b\* coordinates were measured on full-tone patches on each printed sample obtained by different printing pressures. L\*a\*b\* values were also converted to the HEX system (Nazar et al., 2017).

Microscopy of printed elements and measurements of the line width was performed through an Olympus BX51

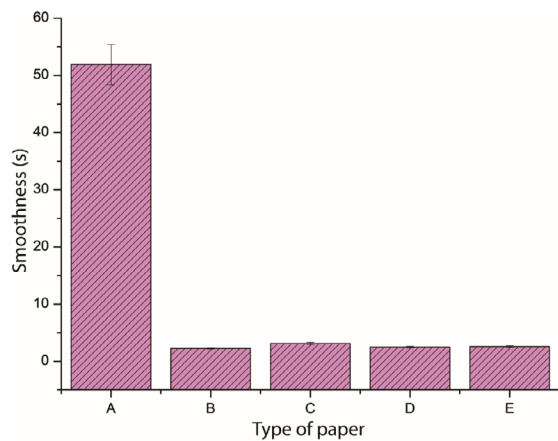


microscope. Obtained images were used for in-software measurements of the width of printed lines, both in positive and in negative. Line measurements were performed at a magnification of 200x, and images of the chosen typographic elements were taken at a magnification of 100x. Five measurements were performed on each print. The 200 µm and 80 µm lines in positive and negative were measured.

## Results and discussion

### Bekk smoothness of papers

The results of the smoothness measurements are presented in Figure 2. All papers except paper A displayed the smoothness under 3.2 s, which is typical for uncoated papers. Paper A displayed average smoothness of 54.72 s. Standard deviation of smoothness measurement for paper A was 7.01, and papers B-E displayed minimal standard deviations of measurements (<0.18).



» **Figure 2:** Bekk smoothness of different recycled paper surfaces

Higher smoothness of paper A compared to other papers means that the printing plate will have to deform less during the engagement in the printing process, and the deformation of the printed elements should therefore be less pronounced than on other papers. Furthermore, the adjustment of the printing pressure on rough papers would be crucial for the optimization of the print's qualitative properties.

### Colorimetric measurements

The colorimetric properties of the prints (CIE L\*a\*b\* values) are presented in Table 2. L\*, a\*, and b\* coordinates of the Pantone 363 U ink are 50.91, -24.88, and 24.05, respectively. Letters A-E present the used papers, and numbers 1, 2, and 3 present the varied printing pressures – 50 N, 150 N, and 400 N, respectively.

**Table 2**

Colorimetric properties of prints obtained by PANTONE 363 U on different recycled papers and by different printing pressure

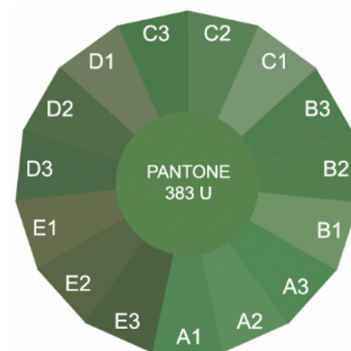
		1	2	3
A	L*	54.81 ± 0.18	51.62 ± 0.24	52.16 ± 0.41
	a*	-24.18 ± 0.22	-25.57 ± 0.23	-26.76 ± 0.17
	b*	19.53 ± 0.13	20.82 ± 0.15	22.19 ± 0.16
B	L*	57.43 ± 0.44	49.65 ± 0.35	48.45 ± 0.37
	a*	-18.89 ± 0.19	-23.96 ± 0.17	-23.68 ± 0.14
	b*	19.96 ± 0.17	22.43 ± 0.19	21.08 ± 0.18
C	L*	59.05 ± 0.32	50.85 ± 0.44	46.55 ± 0.45
	a*	-15.61 ± 0.16	-21.32 ± 0.13	-23.03 ± 0.22
	b*	15.51 ± 0.12	19.28 ± 0.17	19.36 ± 0.21
D	L*	50.31 ± 0.48	42.38 ± 0.41	40.89 ± 0.37
	a*	-8.21 ± 0.11	-15.31 ± 0.22	-16.06 ± 0.23
	b*	15.14 ± 0.16	17.11 ± 0.20	15.72 ± 0.19
E	L*	44.21 ± 0.33	40.95 ± 0.34	38.68 ± 0.28
	a*	-7.12 ± 0.09	-10.72 ± 0.10	-12.72 ± 0.14
	b*	17.56 ± 0.10	16.99 ± 0.14	15.63 ± 0.11

The values in Table 2 indicate that the prints on paper A have the most similar values to Pantone 363 U. All prints on paper A, together with B1 and C1 samples have an increased L\* value compared to the original, which means that the colors are lighter. D1 and E1 samples have the lowest value of a\*, which means that these colors are shifting away from green color. In general, papers D and E present with the highest deviations from the original color. Deviations of each individually printed color from Pantone 363 U are displayed in Figure 3, presented in the HEX system. HEX value for Pantone 363 U is 57844D. LAB color values converted to HEX color system are listed in Table 3.

**Table 3**

L\*a\*b\* values of printed ink on each recycled paper in HEX color system

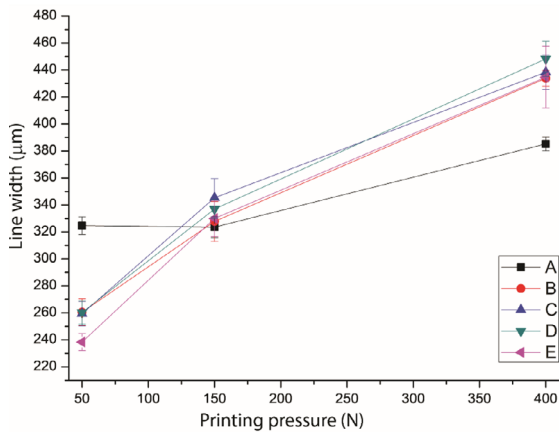
	A	B	C	D	E
1	5F8E60	719366	799672	707C5D	656C4B
2	548756	54814E	5B8357	526B47	576544
3	548854	517E4E	4D794C	4C6846	4D6141



» **Figure 3:** LAB values of printed ink on each paper in HEX color system

## Width of the printed lines

The width of the lines of 200  $\mu\text{m}$  was measured as a representative of the thickest printed line, and 80  $\mu\text{m}$  as a representative of the thinnest printed line. The results of the 200  $\mu\text{m}$  line's width obtained by the varied printing pressure in positive are presented in Figure 4.



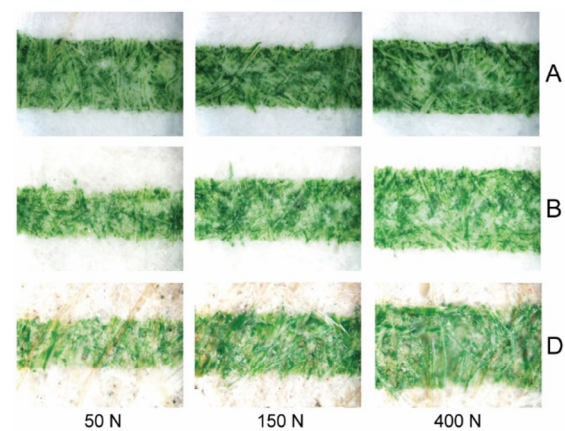
» **Figure 4:** Width of the printed 200  $\mu\text{m}$  line on each paper - positive

Observing Figure 4, one can conclude that paper A is the most constant in comparison to the others in terms of the changes in line width when different printing pressure is applied. This stability can be related to the smoothness of the paper. Since paper A is the smoothest paper among the five used types, the printed ink retains on the surface. Due to the lower smoothness of other papers, printing ink more easily penetrates the pores of the paper (Varepo et al., 2017). Therefore, when the printing pressure is increased, significant changes in the width of the printed lines will occur. At the lowest pressure, the flexible printing plate deforms the least. As the printing pressure increases, the printing plate deforms more, which increases the contact area with the printing substrate, i.e. the printed line becomes thicker. On all papers, the 200  $\mu\text{m}$  line at a minimal pressure of 50 N has a width higher than 200  $\mu\text{m}$ . Although at low pressure there is almost no printing plate deformation, the values for the line width on all papers are higher than they should be because papers are not coated and printed ink is absorbed into and spread on the paper. Therefore, special compensation curves (Tomašegović et al., 2014) should be applied when producing the printing plate intended for print on uncoated recycled papers. A visual comparison of 200  $\mu\text{m}$  lines printed on papers A, B, and D can be seen in Figure 5.

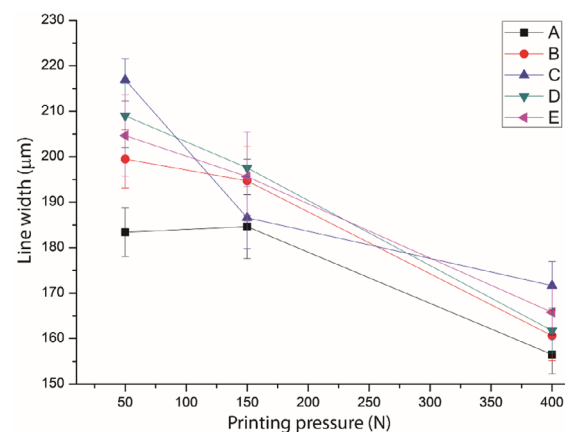
Results presenting the measured width of 200  $\mu\text{m}$  line in negative on each recycled paper after varying the printing pressure can be seen in Figure 6.

For lines in negative, increased printing pressure will result in the thinner line. Only on paper B, a 200  $\mu\text{m}$  line

in the negative can be printed at the lowest pressure of 50 N. At the lowest pressure, the line on paper A presents a value lower than 200  $\mu\text{m}$ , while other papers display higher line widths. Increasing the pressure on papers reduces the width of the line, but paper A is stable in terms of line width decrease at 150 N pressure. 200  $\mu\text{m}$  line can also be achieved on the print on papers B, D, and E when choosing the printing pressure of 150 N. Significant decrease of the line width at 400 N happens due to the expressed deformation of the elastomeric printing plate during the engagement. The deformation increases the contact area between the printing plate and the substrate. In general, when increasing the printing pressure from 50 N to 400 N on chosen substrates, the line width in negative falls by about a quarter of the original value. A visual comparison of 200  $\mu\text{m}$  printed lines in negative can be seen in Figure 7.



» **Figure 5:** Microscopic images of 200  $\mu\text{m}$  line (positive) on papers A, B, and D, magnification of 200x

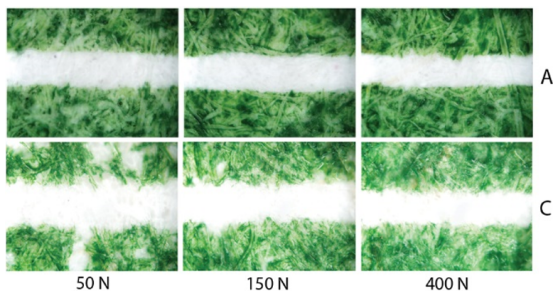


» **Figure 6:** Width of the printed 200  $\mu\text{m}$  line on each paper - negative

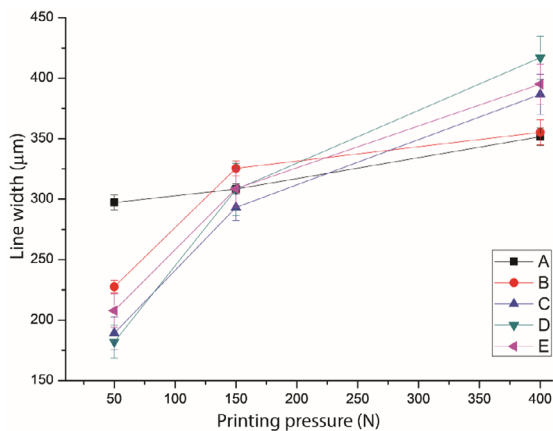
Results presenting the measured width of 80  $\mu\text{m}$  line printed in positive on each recycled paper after varying the printing pressure can be seen in Figure 8.

On all papers, printed lines are wider than 80  $\mu\text{m}$ . Paper D presents with the thinnest line at the lowest pressure

(50 N), but it is twice as wide as it should be. The line on paper A is significantly thicker than on other papers but has the most constant line width when increasing the printing pressure compared to other papers. On paper B, the line presents the smallest change in width when increasing the pressure from 150 N to 400 N, while on paper D, the increase of line width is most expressed. Presented results indicate that a specific compensation curve, different than one intended for printing on paper A, should be applied in the printing plate production process when choosing papers B-E as printing substrates. After the application of the specific compensation curves, printing pressure should be minimized to achieve a fine printed line of the desired width.



» **Figure 7:** Microscopic images of 200  $\mu\text{m}$  line (negative) on papers A, B, and D, magnification of 200x



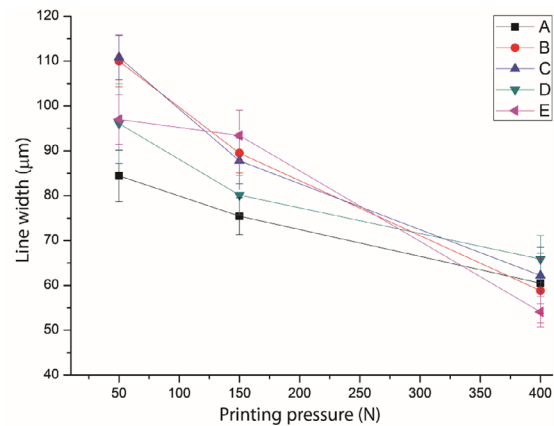
» **Figure 8:** Width of the printed 80  $\mu\text{m}$  line on each paper - positive

Changes in the width of 80  $\mu\text{m}$  line printed in negative on each recycled paper after varying the printing pressure can be seen in Figure 9.

On paper A, at a pressure of 50 N, the lines of 80  $\mu\text{m}$  in negative are slightly wider than they should be but are the thinnest compared to the lines on other papers. As the line pressure increases up to 400 N, the lines become expressively thinner, as expected.

When observing the diagrams presenting the lines in positive (Figures 4 and 8), it can be noticed that paper A

initially (when applying the pressure of 50 N) presents with wider lines compared to other papers. Similarly, lines printed on paper A in negative at 50 N are thinner than on other papers (Figures 6 and 9). This happens because paper A is much smoother than the others. On paper A, printing ink spreads mostly on the surface, even when using the minimal printing pressure, since the pores on the paper are not as large as on other papers. Deviations of line width on all papers are expressed because the papers are uncoated. In the negative, the deviations in the width of each specific line are generally higher than for the lines in positive. The lines in positive are thin, i.e. their surface is small, so the deformation is numerically lower than for the lines in negative, where the printing surfaces are much larger and the "closing" of the line due to the deformation of the printing plate is more pronounced and visible (Mahović Poljaček et al., 2014). Nevertheless, the 80  $\mu\text{m}$  lines in the positive have a significantly higher value than 80  $\mu\text{m}$ . They are similar in value to 200  $\mu\text{m}$  lines. This indicates that most of the tested papers are not suitable for printing very fine elements in positive. However, 80  $\mu\text{m}$  line in negative can be achieved on all papers when choosing the adequate printing pressure.



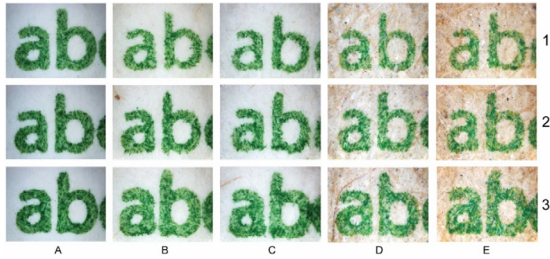
» **Figure 9:** Width of the printed 80  $\mu\text{m}$  line on each paper - negative

## Microscopy of typographic printed elements and determination of color contrast

Microscopic images of typographic elements (18 pt) in positive and negative are presented in Figures 10 and 11, respectively.

In Figure 10, it is visible that paper A presents with the sharpest edges of printed elements at all pressures, and printed elements on this paper have the smallest change in width when the printing pressure changes. The center of the printed letters is the palest – the element edges are outlined- which is usual for the flexographic print due to the printing plate deformation. This happens because

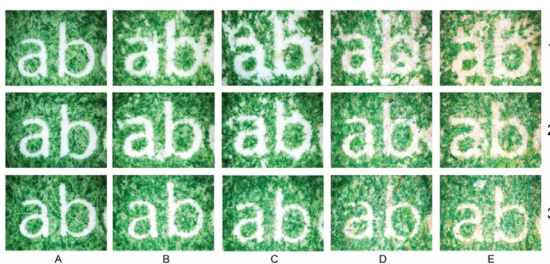
of the different pressure distribution on the finer printing elements on the printing plate during the engagement. Printed elements on all papers are the widest and most filled when applying a printing pressure of 400 N, which reduces the kerning, and some letters could overlap. This is specifically visible on the prints on papers C and E.



» **Figure 10:** Microscopic images of fine printed elements in positive, magnification of 100x

Printing pressure of 50 N on papers C, D, and E results with partially illegible text in the negative (Figure 11). Because of the low printing pressure, the printing plate is not able to deform enough to adjust to the rough printing substrate and the full-tone printed area does not have enough coverage. By increasing the pressure to 150 N the text becomes more legible on all papers, but it is also thinner. Under the pressure of 400 N, due to the deformation of the printing plate, parts of the letters that are already very thin begin to disappear. It is visible that paper A presents with the “cleanest” lines.

It can be concluded that recycled papers D and E are not suitable for the typographic printed elements in negative of higher quality. For papers, A-C, printing pressure should be increased from the standard value of 150 N to achieve the optimal line edge definition and legibility of the typographic elements.



» **Figure 11:** Microscopic images of fine printed elements in negative, magnification of 100x

To determine whether the prints meet the recommendations on the applicability of images and text for the visually impaired (Chung & Bernard, 2018), the color contrasts of the typographic elements on all papers were measured against the background color (Table 4). Various accessibility standards and guidelines prescribe specific difference in luminance between two adjacent colours

or overlaid colours, but commonly indorsed minimal contrast ratio for 18 px texts is 4:1 (Vischeck, 2002).

**Table 4**

Color contrast values concerning the background color (paper) for typographic elements:

	A	B	C	D	E
1	4.41	3.65	3.63	3.12	3.93
2	4.41	3.85	3.89	3.44	4.06
3	3.75	3.89	4.11	3.47	4.10

Minimal color contrast (for a font size of 18pt) was met on all prints except for prints on paper D. For this reason, paper D would not be suitable as a substrate for commercial use for the Pantone 363 U ink used in this experiment. The highest contrast values were achieved on paper A.

## Conclusion

In this research, the optimization of the print quality on different recycled papers was performed. The choice of biodegradable materials as printing substrates for packaging in this experimental work is an optimal solution for the environment. However, there is a difference between recycled papers in terms of their properties, that influence the printability and print quality. For example, their natural shade and rough, porous surface influence the colorimetric properties of the print and ink absorption and spreading.

The results of this research have shown that specific shade of the papers can influence the colorimetric properties of the print to a significant extent, regardless of the increased printing pressure which enables the transfer of more printing ink to the printing substrate. Moreover, the smoothness of the paper is directly related to ink spreading on the surface of the print. Smoothest paper A is most constant in terms of the printed line width when the printing pressure is increased. Fine lines in positive (80 µm) were printed significantly too wide on all papers, even when the lowest pressure of 50 N was chosen. This means that special compensation curves should be applied in the printing plate production process to achieve the adequate width of such fine elements. When printing fine elements in positive, printing pressure should be minimized. Fine lines in negative can be correctly printed on all selected papers by carefully adjusting the printing pressure and achieving the optimal elastic deformation of the printing plate. Furthermore, increased printing pressure can result in the illegibility of the typographic elements in positive, and inadequate pressure in negative could result in unclear edges or disappearing of the printed typographic elements. All recycled papers except paper

D met the minimal color contrast required for the applicability of images and text for the visually impaired.

It can be concluded that most recycled papers used in this experimental work are not suitable for printing very fine elements in positive when choosing flexography as a printing technique. Fine elements in negative can be achieved by carefully adjusting the printing pressure. Since the principles of the sustainable design recommend the minimal needed amount of materials used for the (packaging) product, the consumption of the printing ink should be decreased as much as possible. Therefore, if the maximal possible quality of the print on a recycled paper is crucial, only important fine elements should be designed and printed in negative. Printing pressure should be carefully adjusted to each paper to transfer enough printing ink to achieve legibility, but at the same time to not cause extensive deformation of other printed elements.

## References

- Aydemir, C. (2016) A study on the printability properties of alkali-sized recycled papers. *Science and Engineering of Composite Materials*. 23 (5), 565–571. Available from: doi: 10.1515/secm-2013-0266
- Bates, I., Plazonić, I., Radić Seleš, V. & Barbarić-Mikočević, Ž. (2020) Determining the quality of paper substrates containing triticale pulp for printing industry. *Nordic Pulp and Paper Research Journal*. 35 (2), 272–278. Available from: doi: 10.1515/npprj-2020-0009
- Chung, S. T. L. & Bernard, J. B. (2018) Bolder print does not increase reading speed in people with central vision loss. *Vision Research*. 153, 98–104. Available from: doi: 10.1016/j.visres.2018.10.012
- Cigula, T., Tomašegović, T. & Hudika, T. (2019) Effect of the paper surface properties on the ink transfer parameters in offset printing. *Nordic Pulp and Paper Research Journal*. 34 (4), 540–549. Available from: doi: 10.1515/npprj-2019-0018
- Dahlbo, H., Poliakova, V., Mylläri, V., Sahimaa, O. & Anderson, R. (2018) Recycling potential of post-consumer plastic packaging waste in Finland. *Waste Management*. 71, 52–61. Available from: doi: 10.1016/j.wasman.2017.10.033
- El-Sherif, H. M., Nasser, A. M., Hussin, A. I., Abd El-Wahab, H., Ghazy, M. B. M. & Elsayed, A. E. (2019) Tailoring of mechanical properties and printability of coated recycled papers. *Polymer Bulletin*. 76 (6), 2965–2990. Available from: doi: 10.1007/s00289-018-2515-7
- IGT Testing Systems (2016) *F1 Basic*. Available from: <https://www.igt.nl/product/f1-basic/> [Accessed: 26th September 2020].
- Ivanković, A., Zeljko, K., Talić, S. & Lasić, M. (2017) Biodegradable Packaging in Food Industry. *Jurnal of Food Safety and Food Quality*, 68 (2), 23–52. Available from: doi: 10.2376/0003-925X-68-26
- Izdebska, J., Żołek-Tryznowska, Z. & Świętoński, A. (2015) Correlation between plastic films properties and flexographic prints quality. *Journal of Graphic Engineering and Design*. 6 (2), 19–25.
- Kaiser, K., Schmid, M. & Schlummer, M. (2017) Recycling of Polymer-Based Multilayer Packaging: A Review. *Recycling*. 3 (1), 1–26. Available from: doi: 10.3390/recycling3010001
- Mahović Poljaček, S., Tomašegović, T., Cigula, T., Gojo, M. & Milčić, D. (2014) Formation of the Printing Elements in the Photopolymer Material Used in Flexography. *Key Engineering Materials*. 611–612, 883–891. Available from: doi: 10.4028/www.scientific.net/KEM.611-612.883
- Marrez, D. A., Abdelhamid, A. E. & Darwesh, O. M. (2019) Eco-friendly cellulose acetate green synthesized silver nano-composite as antibacterial packaging system for food safety. *Food Packaging and Shelf Life*. 20, 100302. Available from: doi: 10.1016/j.fpsl.2019.100302
- Miljković, P., Valdec, D. & Matijević, M. (2018) The impact of printing substrate on dot deformation in flexography. *Tehnički Vjesnik*. 25 (2), 509–515. Available from: doi: 10.17559/TV-20170710152140
- Mohamed, R. M. & Yusoh, K. (2015) A Review on the Recent Research of Polycaprolactone (PCL). *Advanced Materials Research*. 1134, 249–255. Available from: doi: 10.4028/www.scientific.net/amr.1134.249
- Moustafa, H., Youssef, A. M., Darwish, N. A. & Abou-Kandil, A. I. (2019) Eco-friendly polymer composites for green packaging: Future vision and challenges. *Composites Part B: Engineering*. 72, 16–25. Available from: doi: 10.1016/j.compositesb.2019.05.048
- Mraović, M., Muck, T., Pivar, M., Trontelj, J. & Pleteršek, A. (2014) Humidity Sensors Printed on Recycled Paper and Cardboard. *Sensors*. 14 (8), 13628–13643. Available from: doi: 10.3390/s140813628
- Nazar, M., Khan, R. Q., Perveen, M. & Khan, W. Q. (2017) Web branding harmonizer: Need of color harmonies and its solution in website development. In: *2017 International Conference on Infocom Technologies and Unmanned Systems (Trends and Future Directions) (ICTUS)*. 18–20 December 2017, Dubai, United Arab Emirates. IEEE, pp. 346–350. Available from: doi: 10.1109/ICTUS.2017.8286030
- Pivnenko, K., Eriksson, E. & Astrup, T. F. (2014) Waste paper for recycling: Overview and identification of potentially critical substances. *Waste Management*. 45, 134–142. Available from: doi: 10.1016/j.wasman.2015.02.028
- Tomašegović, T., Mahović Poljaček, S., Cigula, T., Gojo, M. & Milčić, D. (2014) Correlation between the lams and printing element area on the flexographic printing plate. In: Urbas, R. (ed.) *Proceedings of 7th Symposium of Information and Graphic Arts Technology, 5-6 June 2014, Ljubljana, Slovenia*. University of Ljubljana, Ljubljana. pp. 43–49.

- 
- Tomašegović, T., Beynon, D., Claypole, T. & Poljaček, S. M. (2016) Tailoring the properties of deposited thin coating and print features in flexography by application of UV-ozone treatment. *Journal of Coatings Technology Research*. 13, 815-828. Available from: doi: 10.1007/s11998-016-9794-4
- Tomašegović, T., Mahović Poljaček, S., Stržić Jakovljević, M. & Urbas, R. (2020) Effect of the Common Solvents on UV-Modified Photopolymer and EPDM Flexographic Printing Plates and Printed Ink Films. *Coatings*. 10 (2), 136. Available from: doi: 10.3390/coatings10020136
- Varepo, L. G., Brazhnikov, A. Y., Volinsky, A. A., Nagornova, I. V. & Kondratov, A. P. (2017) Control of the offset printing image quality indices. *Journal of Physics: Conference Series*. 858 (1), 12038. Available from: doi: 10.1088/1742-6596/858/1/012038
- Vischeck (2002) *About Vischeck*. Available from: <http://www.vischeck.com/vischeck/> [Accessed: 26th September 2020].
- Wienke, A., Hoffmann, G.-A., Koch, J., Jäschke, P., Overmeyer, L. & Kaierle, S. (2020) Ablation and functionalization of flexographic printing forms using femtosecond lasers for additively manufactured polymer-optical waveguides. *Procedia CIRP*. 94, 846–849. Available from: doi: 10.1016/j.procir.2020.09.112
- X-Rite (2018) *eXact Standard Handheld Spectrophotometer*. Available from: <https://www.xrite.com/categories/portable-spectrophotometers/exact> [Accessed: 26th September 2020]

